Molecular Dynamics Simulation of Forsterite and Magnesite Mechanical Properties: Effect of Carbonation on Comminution Energy

Akash Talapatra

Thesis submitted to the faculty of Virginia Tech in partial fulfillment of the requirements for the degree of

Master of Science

In

Mining Engineering

Bahareh Nojabaei, Chair

Rohit Pandey

Fatemeh Molaei

May 02, 2024

Blacksburg, VA

Keywords: Mineral Carbonation, Communication Energy, Stress-strain Relationship, Elastic Properties, Radial Distribution Function.

Molecular Dynamics Simulation of Forsterite and Magnesite

Mechanical Properties: Effect of Carbonation on Comminution Energy

Akash Talapatra

Technical Abstract

This research describes the mechanical behavior of forsterite and magnesite, two common geomaterials at the molecular level. Through comprehensive analysis, we investigated how varying thermodynamic and physical conditions influence the stress-strain relationships of these crystalline structures. Employing molecular scale studies on three-dimensional models of forsterite and magnesite, we examined the effects of different temperatures (300K, 500K, and 700K) and strain rates (0.001, 0.01, and 0.05 ps^{-1}) on initiating deformation under both tensile and compressive forces.

Our observations indicate that at elevated temperatures, these monocrystals undergo deformation at lower stress levels. Specifically, Young's modulus of forsterite and magnesite under tensile force approximates 154.74 GPa and 92.84 GPa, respectively, while under compressive force, these values are around 120.45 GPa (forsterite) and 77.04 GPa (magnesite). We noted a reduction in the maximum strength of the crystalline structures with increasing temperature.

Furthermore, we examined the influence of strain rate sensitivity and grain size on the materials' properties. Decreasing grain sizes resulted in a drop in yield strengths of forsterite and magnesite by 7.89% and 9.09%, respectively, compared to initial systems. Additionally, we investigated changes in elastic properties under various pressures and temperatures, revealing significant alterations in the materials' behavior.

Moreover, analysis of the radial distribution function (RDF) unveiled differences in pairwise interactions between atoms, with the peak intensity of Si-O interactions surpassing that of Mg-O. This observation suggests variations in bonding strengths within the materials, influencing their overall mechanical behavior.

Lastly, our findings indicate that magnesite exhibits favorable properties for the comminution process, a result of mineral carbonation on forsterite. This study provides valuable insights into the complex interplay between mineral composition, physical conditions, and mechanical behavior, offering potential implications for industries reliant on these geomaterials.

Molecular Dynamics Simulation of Forsterite and Magnesite Mechanical Properties: Effect of Carbonation on Comminution Energy

Akash Talapatra

General Audience Abstract

Mineral carbonation contributes to CO_2 reduction, and it may also reduce the cost of mineral processing by improving the mechanical properties of rock/ore. Here, we study and compare the mechanical properties of two minerals, forsterite (Mg_2SiO_4) and magnesite ($MgCO_3$) using molecular dynamics (MD) simulation. The goal is to understand whether carbonation results in hardness reduction of rock and subsequently comminution energy during the crushing and processing of the ore. We investigated how these materials respond to different physical conditions, such as temperature and strain rate, to understand their behavior under stress. By examining the molecular structure of forsterite and magnesite at temperatures ranging from 300K to 700K and strain rates of 0.001, 0.01, and $0.05ps^{-1}$, we observed how they deform when subjected to both tensile and compressive forces.

This study has shown that at higher temperatures, both forsterite and magnesite monocrystals undergo deformation more easily under pressure. Forsterite is found relatively hard and shows maximum strength before deformation compared to magnesite. The stiffness of magnesite decreases at elevated temperatures which reduces the energy requirement for the comminution process. We also looked at how pressure and temperature changes affected their elasticity.

Ultimately, our findings suggest that magnesite may be more suitable for processes like comminution, which involves breaking down materials, compared to forsterite. This insight into

the effects of mineral carbonation on geomaterials contributes to our understanding of how these minerals behave under different conditions and could have implications for various industries.

Dedication

With deep gratitude, this work is dedicated to my beloved family. To my parents, whose boundless love and unwavering support have been the cornerstone of my journey. Their support and encouragement have shaped me in ways I can never fully express. To my friends who became my supporters and helped with any problem I faced. They encouraged me to finish this important research in time. They also give me inspirational messages every time. In humble acknowledgment, I extend my heartfelt thanks to God for blessing me with his grace.

Acknowledgments

First and foremost, I am deeply grateful to my supervisor, Dr. Bahareh Nojabaei, whose unwavering encouragement and guidance have been instrumental throughout my graduate studies. Her constant interest and genuine interest in my success have been a constant source of inspiration. I am indebted to her for her commitment, advice, and unwavering support, which have been pivotal in achieving my academic goals.

I extended my heartfelt thanks to my esteemed committee members Dr. Rohit Pandey and Dr. Fatemeh Molaei, for their constant support, suggestions, and great ideas that enabled me to complete this work. I would like to express my gratitude to Dr. Fatemeh Molaei, who trained me, taught me how to use the LAMMPS, and whose input and skills in molecular dynamics simulations were extremely helpful.

Special gratitude is reserved for the Mining and Minerals Engineering Department, whose provision of essential resources and facilities has been indispensable to my research. I am particularly grateful to Warren Lucero for his technical assistance and equipment maintenance. The supportive environment fostered by the department's faculty, staff, and fellow students has been invaluable, especially during challenging times. I am thankful for the scholarships provided by the WAAIME Division of SME and extend my gratitude to Lyda Hull and Carol Trutt for their financial support.

Finally, I extend my heartfelt thanks to my friends and lab mates, whose support and encouragement have enriched my academic journey. Special thanks to Festus Animah, Nestor Santa, August Greth, Augustine Effiong, Salman Karim, Abduljeleel Ajibona, Uzezi Orivri, and

James Frimpong for their friendship, guidance, and encouragement. Their constant support has been a source of strength and inspiration, for which I am profoundly grateful.

Table of Contents

List of Figures

List of Tables

Chapter 1 – Introduction

Mineral carbonation is an emerging approach of capturing CO_2 from the surrounding environment and storing it in the form of carbonate minerals. This mineralization particularly occurs in the calcium, magnesium, and silicate-rich rocks/geomaterials (wollastonite, and serpentine) that compose the earth's upper mantle. This process has been done during the weathering of those rocks/geomaterials [1], [2]. The major pathways and kinetics of capturing and storing enriched CO_2 in carbonate minerals have been described frequently as research agenda to discuss the potential and required cost of this process. Researchers have not only focused on the potential of mineral carbonation in minimizing greenhouse gas emissions and assuming the storage is nontoxic and permanent. They also have been searching for emulating and accelerating spontaneity as well as the balance of this process within the earth's deep interior[3], [4], [5].

Mineral carbonation signifies a chemical process whereby carbon dioxide (CO_2) interacts with minerals rich in alkaline and alkaline-earth-bearing minerals (magnesium and silicate rich) minerals to form stable carbonate minerals[6]. A wide variety of silicate minerals groups containing Ca^{2+}, Mg^{2+}, and Fe^{2+} ions present like targeting mineral carbonation are olivine, serpentine, pyroxene, mica group, and clay minerals. However, past work has claimed that olivine group minerals, particularly forsterite (Mg_2SiO_4) are the most potential feedstock for the mineral carbonation process and form stable carbonate minerals ($MgCO_3$). It is a common mineral in ultramafic rocks and is formed because of the cooling and solidification of magma. That's why it is much more stable at higher temperatures and pressures[7]. Besides, forsterite has a higher surface area to volume ratio, for which CO_2 is highly reactive to the forsterite[8], [9]. In addition, Xu et al. (2000) investigated the complete alteration of the primary minerals to specify the

maximum quantity of CO_2 sequestrated by each mineral and found that the olivine group minerals (forsterite) have a CO_2 sequestration potential around 2014.70-1896.30Kg/m^3 (Table 1) [10].

On the other hand, magnesite is a carbonate-rich mineral found in the tectonically active regions and comprises the earth's lower mantle. It's formed from the hydrothermal alteration of olivine group minerals from ultramafic rocks. That's why it is less stable at higher temperatures and pressures [11]. Figure 1 shows a schematic view of the 3D atomic and crystalline structures of forsterite and magnesite. Both minerals are considered crystals: forsterite crystalizes in orthorhombic, and magnesite crystalizes cubic systems. The consideration of crystal orientation and lattice parameters is also provided in the later section.

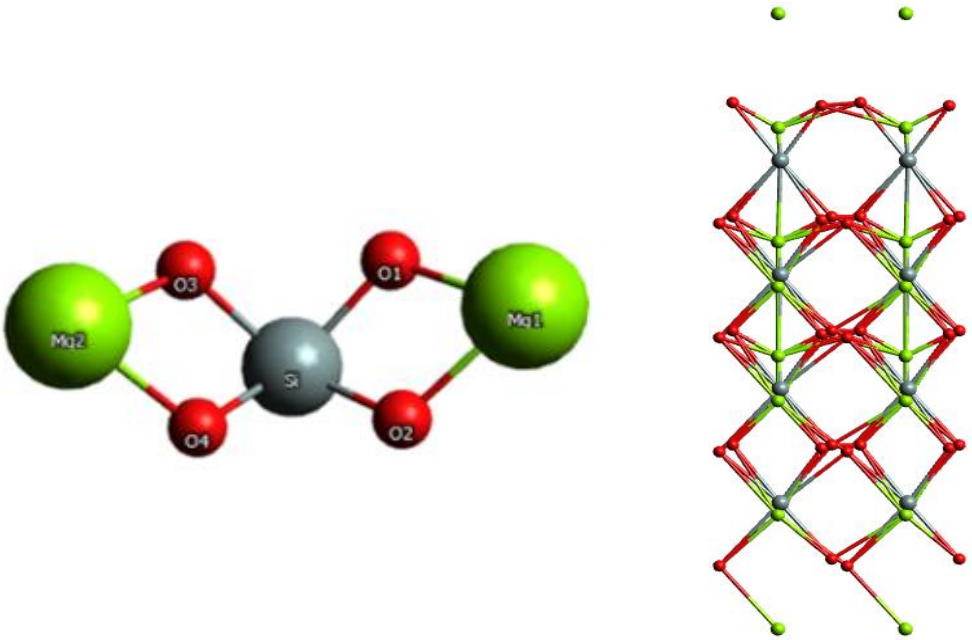

(a)

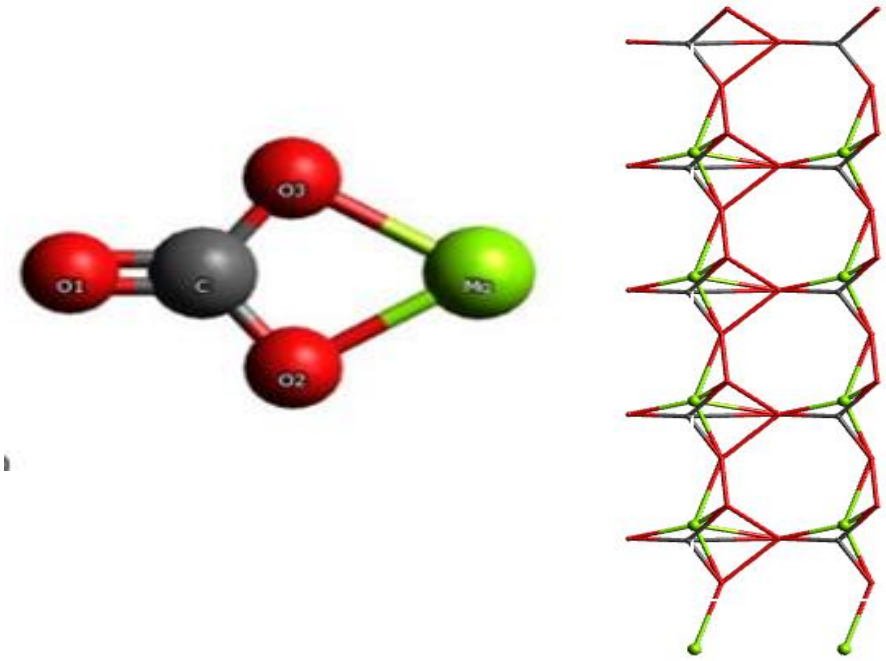

(b)

Figure 1: 3D atomic and crystal structure of forsterite (a) and magnesite (b).

The mineral carbonation reaction between forsterite and CO_2 is expressed as follows:

$$Mg_2SiO_4 + CO_2 \rightarrow MgCO_3 + SiO_2 \quad \text{.....(1)}$$

Table 1: CO_2 sequestration potential of major rock-forming minerals[10].

Mineral Name	**Formula**	**Potential CO_2 Fixed, Kg/m^3 mineral**
Olivine group (forsterite)	Mg_2SiO_4- Fe_2SiO_4	2014.7-1896.3
Pyroxene group (enstatite)	$(Mg, Fe)_2 Si_2O_6$	1404
Serpentine	$Mg_3Si_2O_5(OH)_4$	1232
Wollastonite	$CaSiO_3$	1097.1
Amphibole group (hornblende)	$Ca_2Na_{0-1}(Mg.Fe(II)_{3-5}(Al.Fe(III)_{2-0}[Si_{6-8}Al_{2-0}O_{22}](O,OH)_2$	1000.4
Mica group (biotite)	$K_2(Mg,Fe(II))_{6-4}(Fe(III),Al)_{0-2}[Si_{6-5}Al_{2-3}O_{20}](OH)_{4-2}$	671
Plagioclase (anorthite)	$Ca[Al_2Si_2O_8]$	436.4
Clay Minerals	$(1/2Ca,Na)_{0.7}(Al,Mg,Fe)_4(Si,Al)_8O_{20}(OH)_4.nH2O$	161.2

(smectite)

As mentioned before, mineral carbonation occurs naturally in silicate rocks (alkaline/alkaline-earth minerals) when a higher concentration of CO_2 (3.08%) is brought into contact with those minerals. This carbonation process can occur in both in-situ and ex-situ reservoir conditions. These two processes differentiate based on the time scale and contact of CO_2 [12]. In situ carbonation involves the injection of CO_2 into the geological formation containing silicate minerals (forsterite) to form solid carbonate minerals (magnesite). It's an ongoing process that runs for a long geologic time scale and stores the formed magnesite permanently in the subsurface. It is conducted for different geological settings including ultramafic rocks. Basalt rocks, etc. It exploits the chemical potential energy inherent in the active tectonic exposure mantle forsterite at the earth's surface, does not require extensive transport, and treatment of solid reactants, and requires less energy for maintaining the geological conditions [13], [14]. Contrary, ex-situ carbonation involves the reaction of forsterite with CO_2 in a controlled environment. This process occurs above the ground within a separate reactor and industrial process, and typically, takes place over a period of hours to days [15]. The CO_2 used for the ex-situ carbonation process usually comes from coal-fired, power plants, steel mills, cement factories, etc. [16]. In addition, silicate minerals are brought from industrial wastes as forms of fly ash, cement kiln dust, steel slag, etc. which can sequestrate around 200-300 Mt of CO_2 annually [15], [17]. This process sequesters a large amount of CO_2 and produces reusable, valuable, and stable carbonate materials for different industrial purposes (Figure 2a) [12]. However, both in-situ and ex-situ mineral carbonation processes are part of carbon-negative solutions and have a great potential to reduce the effect of CO_2 on the environment (Figure 2b) [18].

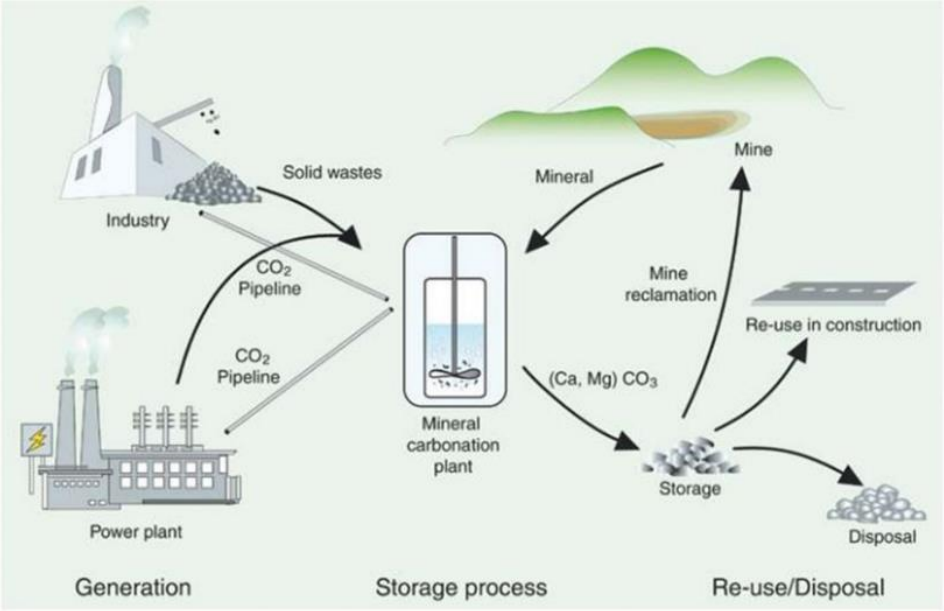

(a)

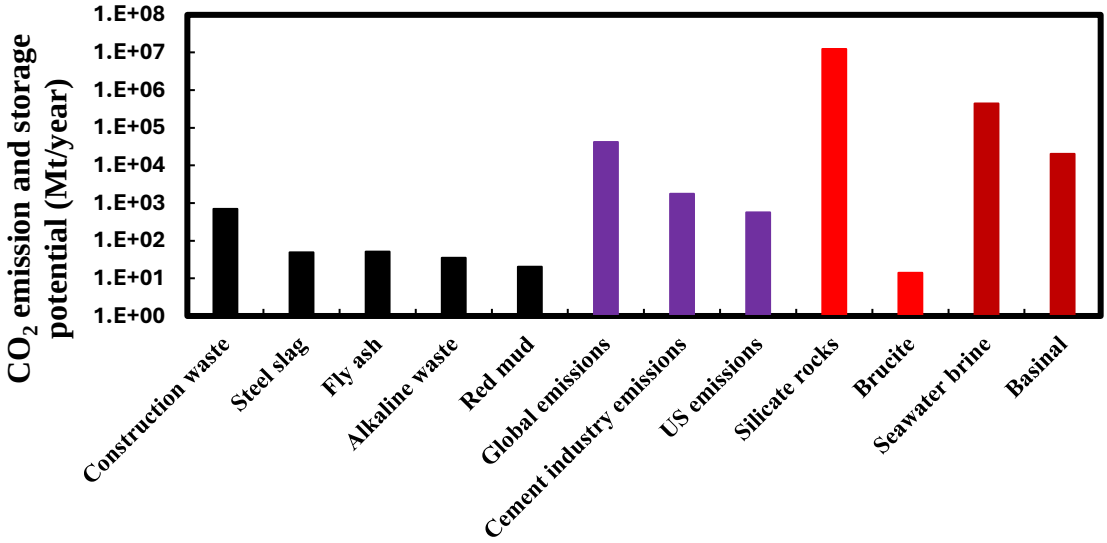

(b)

Figure 2: (a) A schematic view of the carbonation process of silicate rocks or industrial residues [10]. (b) Global Capacity to sequestrate CO_2 via mineralization [19].

However, this carbonation or chemical weathering process on forsterite minerals makes it less reactive with a higher surface area-to-volume ratio. This causes the surface area of the forsterite, which acts as the dissolved phase, liberating Mg^{2+} ions into the solution, consequently augmenting

the supersaturation concerning the magnesite [19]. These changes in the surface area also impact the activation methods and reactivity efficiency of the mineral during the pretreatment process (such as thermal treatment). Besides, carbonation can impact the compressibility of mineral feedstock by changing the density, porosity, and size distribution properties. Since the changes in these properties are also correlated with changes in the physical properties of minerals, it becomes crucial to study whether the carbonation process impacts the energy input requirements for particle size reduction or not. This size reduction process of minerals is called the comminution process. It is a physical pre-treatment method in mineral processing involving ore size reduction (such as mineral crushing, grinding, and breaking the minerals into smaller/finer particles). It is a critical component for the mineral processing flowsheet before converting the ores into smaller particles to be separated from waste rocks. It involves increasing the surface area of the ore (separation) for chemical reaction, liberating the valuable mineral from the ores (liberation), reducing the particle size to meet product specifications (concentration), and collecting the crushed particles by grades (sorting optimization) [12], [20]. During the comminution process, the formation of minerals, mineral structure, presence of defects, mechanical strength, and grain size plays a great role. Because, for crushing and grinding of particles, the comminution process requires significant external energy input to break the particles. The carbonation process has changed the surface chemistry of minerals and minerals coated with carbonates have a different sensitivity [21], [22]. However, explaining these reactive phenomena in the flotation process from a chemical perspective is not within the scope of this study. Rather, this research focuses on the changes in physical properties before and after the carbon process on silicate-rich minerals.

The hardness and strength properties of the minerals depend on the crystalline structure, 3D arrangement of the atoms, and interatomic behavior of minerals. The interatomic structures in

crystals are alternated by the carbonation process [23]. Till now, few studies have been performed on the strength properties of the forsterite and magnesite individually. Holyoke et al. (2014) experimented on two different types of magnesite aggregation (coarse and fine grains) to determine the triaxial deformation over a wide range of grain sizes (1μm to 100μm), temperatures (400-1000^{o}C) and strain rates (2×10^{-7} s^{-1} to 2×10^{-4} s^{-1}). Experiments were conducted on fine-grained magnesite using a Heard gas confining medium rock deformation apparatus, maintaining a consistent effective pressure of 300 MPa. Similarly, coarse-grained magnesite underwent experimentation in a Griggs piston-cylinder rock deformation apparatus, with a steady effective pressure of 900 MPa. In both aggregation types, the strengths of the magnesites at higher temperatures were reduced. Both fine and coarse-grained magnesites showed little chance of strain recovery or recovery of the minerals' structure or properties after deformation. That study also mentioned that as temperatures rise, magnesite's strength diminishes due to shifts in deformation mechanisms, indicating a physical rather than chemical change in its behavior. [24]. In another study, Liu et al. (2016) carried out an atomic simulation (using a transferable empirical interatomic potential) to investigate the structural and elastic properties of the magnesite over a wide range of pressure (based on the earth's mantle condition). The simulation work found that magnesite shows anisotropic behavior at lower mantle depth, but significant change with increasing depth. The percentage anisotropy in the shear and compressibility were calculated for a pressure range from 0 to 150 GPa and observed that at higher pressure (≥120GPa), both shear and compressibility values were close to 1 (0 means isotropic and 1 means anisotropic). This observation suggested that as pressure increases toward the upper limit of the studied range, magnesite shear and compressibility properties become more anisotropic behavior [25]. Yao et al. (2018) worked on the impacts of pressure and temperature on the magnesite (considering local density

approximation) using the first principal calculation. All the pressure and temperature values were in lower mantle conditions. The authors found the elastic and thermodynamic properties of magnesite were influenced by the residual motion of particles even at absolute zero due to the quantum uncertainty principles (known as zero-point motion) at increasing temperatures. They also noticed a change (around 4.0%) in the shear and bulk modulus from static to ambient conditions (300K and 0 GPa) [26]. On the other hand, Gonzalez et al. (2018) investigated the structural, dielectric, and vibrational spectroscopic properties of the amorphous form of forsterite. The work had been done in two approaches: classical molecular dynamics (MD) for structural evolution using the empirical charged-based rigid ionic model and density functional theory (DFT) for measuring electronic structure using quantum mechanics. It also stated the degrees of freedom for the disordering in crystal structure for higher temperatures (400K to 2000K) [27]. In 2019, Gouriet et al. (2019) investigated the mechanical deformation of the orthorhombic structure of forsterite for applied strains. They determined the energy-strain curves and linear elastic regimes to figure out the ultimate instability of the crystal structure. The maximum stress values from stress-strain curves were found near 15.9, 12.1, and 29.3GPa along the different crystallographic (001), (010), and (100) directions, respectively. They also observed a similar change of features in ideal shear stress in each direction, firstly showing the weakest shear followed by a change in stiffness before and after deformation [28]. In addition, Choudhary et al. (2020) studied the mechanical stability and degradation of forsterite and noted that the increasing content of forsterite increased the mechanical strength of the composite compared to the calcium phosphates and calcium silicates [29].

Till now, no studies have been done to study the impact of mineral carbonation on the mechanical properties of forsterite and magnesite in various conditions (temperature, pressure, and applied

forces). This present work focuses on the evolution of the stress-stain relationship according to the changes in the physical properties. The effect of temperatures, loading rates, and grain sizes on the maximum stress values of two different minerals was studied. In addition, the mineral that is highly sensitive to the applied forces is also measured. The changes in pressure and thermal effects on the elastic properties are observed for the two minerals. Later, the radial distribution function is also evaluated for measuring the pairwise interaction between the Si-O and C-O bonds. This study compares the strength properties and microstructure of the two minerals under the same conditions. This study does not consider any observation from the reaction kinetics during mineral carbonation.

1.1. Motivations

Understanding the motivations behind the study of olivine-rich minerals, particularly forsterite, is essentially for appreciating their potential applications in carbon sequestrations and other fields. This section explores the key reasons driving research and applications in this field.

- Carbon dioxide sequestration: The olivine-rich mineral (Forsterite) has a high capacity to react with CO_2 making it a promising technique for long-term CO_2 sequestration to mitigate climate changes.
- Abundance and availability: Olivine-rich mineral (forsterite is a naturally abundant mineral, making it a readily available and cost-effective option for the carbon sequestration process.
- Scientific curiosity: Investigating the fundamental mechanical behavioral changes in forsterite minerals before and after the carbonation process can contribute to the broader knowledge of rock geomechanics.
- Energy Savings potential: We investigate whether mineral carbonation reduces the energy requirements for the comminution process, a method involving size reduction

and mineral liberation. Throughout this research, we assess if breaking down of magnesite is less energy-intensive than that of forsterite.

1.2. Thesis Scope

This study compares the strength properties of the two geomaterials (forsterite and magnesite) in various thermodynamic conditions, to assess the effect of mineral carbonation on comminution energy for mineral processing. The work focused on the molecular dynamics (MD) simulation method using appropriate potential and necessary forcefield parameters. Firstly, the stress-strain behavior is investigated by allowing the deformation of those monocrystals using tensile as well as compressive force in the axial direction. The deformation has been done under different temperatures and strain rates for both applied forces.

Then, the impact of strain rate sensitivity (SRS) on those materials' stability during the deformation is highlighted to understand the deformation behavior of minerals and measure the changes in yield pressure. To demonstrate the effect of SRS on materials' strength and stability different temperatures and strain rates are used, following the comparison between them showing varying levels of sensitivity, influencing their stability and strength. The later section investigates the influence of grain size on those two monocrystals, emphasizing the role of grain boundaries in resisting deformation and affecting material strength and ductility. By examining the morphology, size distribution, and nature of grains and their boundaries, valuable insights into the mechanical behavior of crystals are gained.

The next section delves into the significance of elastic properties in understanding materials for geophysics and geochemistry, crucial for inspecting the earth's interior. By analyzing the relationship between stress and deformation, valuable insights into material structure and behavior

are gained. Through pressure and temperature-dependent analysis, it's revealed how these properties influence material strength and phase transitions, offering key insights for interpreting geophysical data and designing materials for specific conditions.

The last section determines the pairwise interactions and coordination numbers within mineral structures, known as the radial distribution function. By analyzing the distribution of neighboring particles around a central particle, RDF provides insights into material homogeneity and equilibrium.

1.3. Objectives

In this study, we have investigated the effect of mineral carbonation on the physical properties of silicate minerals. Our objectives span various facts of this phenomenon, each contributing to a comprehensive understanding of its behavior. The main objectives of this study are as follows:

- Investigate the changes in stress-strain relation of forsterite and magnesite at different temperatures and applied strain rates.
- Analyze the microstructure of increasing causing he forsterite and how it impacts the internal arrangement of rock constituents.
- Investigate the strain rate sensitivity of forsterite and magnesite to applied forces and strain rate.
- Investigate the effect of temperature and pressure on the elastic properties of forsterite and magnesite.
- Investigate the pairwise interaction between the silicon-oxygen bond and carbon-oxygen bond.

In summary, this thesis work aims to explain the changes in the mechanical properties of minerals using a computational approach. By achieving these objectives, we contribute valuable insights to sustainable materials science and environmental engineering.

Chapter 2 – Methodology

2.1. Molecular Modeling and Forcefield Parameters

Molecular dynamics (MD) simulation provides a basic representation and interpretation of molecular interaction modeling of any material with detailed information and underlying governing mechanisms. It is a powerful tool for studying particle movement, mechanical behavior, and other properties according to the materials' physical phenomena and chemical reaction kinetics[30]. As a part of solid dynamics, it measures the material's deformation, elasticity, diffusion, yield, and other physical behavior at the atomic level. It can predict the dynamics of materials' behavior under different temperatures and loading conditions. This predictive capacity in atomic and molecular scales follows the validation of computational modeling experiments. The noticeable things are the flexibility of working with different sizes of materials and visualization of the molecular interaction at the atomic scale which might not be possible in experiments. The fundamental theory of molecular dynamics simulation is to observe the dynamic trajectory of an atomic system and analyze the atomic interactions among the respective atoms. Those phenomena follow and solve Newton's equation of motion (F=ma, where F= vector of force, m=mass, and a= acceleration). Prior works on different materials using molecular dynamics simulation have offered reliable outputs for illustrating their mechanical properties [31], [32]. A molecular dynamics simulation study on forsterite and magnesite minerals has also been performed using a Large-scale Atomic/Molecular Massively Parallel Simulator (LAMMPS) software package. To

conduct molecular dynamics simulations for investigating the mechanical properties of these two minerals, LAMMPS is considered an efficient parallel platform [33].

However, better performance of molecular dynamics simulation depends on the implementation of a suitable and successive potential for those crystals. Since the model's reliability and validation directly depend on this selected potential, the main task of the molecular dynamics work is to use the right forcefield parameters to obtain accurate results and configuration. The accessibility of the interatomic potential to the size of the system is a governing factor for the numerical integration of the above equation. Here, in this study, an empirical potential model 'Buckingham' potential is used for simulating the atoms of both crystals [34]. This potential is freely available with the LAMMPS library package. It substantially considers the long-range electrostatic terms with classical Coulombic energy, a short-range repulsive term, and a three-body harmonic term. This potential is a bond order and short-range interaction-based potential which is attributed to the partial charge of the atoms. Several prior studies used this potential to reproduce the structural properties of both forsterite and magnesite crystals [35], [36]. This Buckingham potential can be expressed as follows:

$$E = A_{ij}.e^{-\frac{r_{ij}}{\rho_{ij}}} - \frac{C_{ij}}{r_{ij}^6} \quad \text{..... (2)}$$

$$E = \frac{Cq_iq_j}{\epsilon r_{ij}} \quad \text{..... (3)}$$

where, E= potential energy, A= energy units, e= elementary charge, ρ= distance units, C= energy-distance^6 units, r= distance between the one ion type (i) and another ion type (j) less than cutoff distance (i,j= Mg, Si, C, and O) and $q_{i/j}$= partial charges for a particular atom. Though Buckingham potential seems simple, this potential considers the pair ion charges, thermal expansion, heat

capacity, and long-range coulombic interaction to illustrate the short-range interaction between the paired atoms. For this reason, the Buckingham potential is more computationally intensive and time-consuming to calculate compared to other interatomic potentials commonly used for silicate and carbonate molecules. This is because it considers additional factors like thermal expansion and heat capacity, which adds complexity to the calculations. As a result, simulations using the Buckingham potential will run slower and require more computational power than those using simpler potentials. The performance of this potential depends on the forcefield parameters of the forsterite and magnesite. The initial configuration and those forcefield parameters are shown in Tables 2 and 3, respectively.

In this study, Moltemplate was used to generate simulation models for forsterite and magnesite [37]. It is particularly a cross-platform text-based molecular builder (for coarse-grained molecular models) made for LAMMPS. The simulation models of these two crystals were made with random orientation of the crystals as well as using the Voronoi method including random seeds [34]. The conjugate gradient (CG) algorithm was used to optimize the initial structure and position of the atoms [38]. This minimization algorithm adds the force gradient to the previous iteration information to compute the new direction perpendicular to the previous search iteration.

Table 2: Selected materials and atomic model properties.

Material Type	**Dimension (Å)**	**Potential**	**Number of Atoms**	**Atomic Bond Type**	**Lattice Constant (Å)**	**Crystal System**
Forsterite (Mg_2SiO_4)	50×50×50	Buckingham	4480	Ionic-Covalent	a = 4.787 b =10.272 c = 6.023	Orthorhombic
Magnesite ($MgCO_3$)	49×49×49	Buckingham	4250	Ionic-Covalent	a = 4.64 b = 4.64 c = 14.93	Trigonal

Table 3: Forcefield parameters used in this study.

Buckingham Potential			
Ion Pairs	A(eV)	B(Å)	C(eVÅ^6)
Mg-O	1428.5	0.2945	0.0
Si-O	473.2	0.4157	0.0
O-O	22764.3	0.1490	60.08
C-O (Morse)	4.71	3.80	1.18
Harmonic 3-Body Term			
	k(eVrad^{-2})	Θ_0 (degrees)	
O-Si-O	2.09	109.47	
O-C-O	1.69	120.0	
Charges			
Mg	+2.00		
Si	+4.00		
C	+1.135		
O (for forsterite)	+0.84819		

Table 4: Density of materials.

Density	**Forsterite**	**Magnesite**
MD Simulation	3.08	2.94
Experimental	3.33	3.1

2.2. Simulation Conditions and Procedures

For the starting of simulation procedures, The Verlet algorithm was used with a timestep of 1fs to calculate the dynamic trajectories of the particle. The long-range Coulombic interaction was calculated using the Ewald summation method. Two different systems were approached to an equilibrium state under a specified temperature (300K) using an NPT ensemble under zero pressure in all directions. Nose-Hoover thermostat and Barostat were used to control the temperature and pressure successfully. Periodic boundary conditions were applied in each

direction of the simulation box. The forces were applied to the systems by altering the length of the simulation box along the direction of strain application. The time step is set to 1 fs, totaling 40000 steps, meaning that tensile strain is applied until the length of the simulation box in the strain direction reaches 1.5 times its initial value. A strain rate is selected at 0.01 ps^{-1} initially to compare our results with the previous work. The visualization of the models after the equilibration and elongation is shown in Figure 3. The details about applied equations, parameters, and different thermodynamic and loading condition conditions are described in each subsection of the results section.

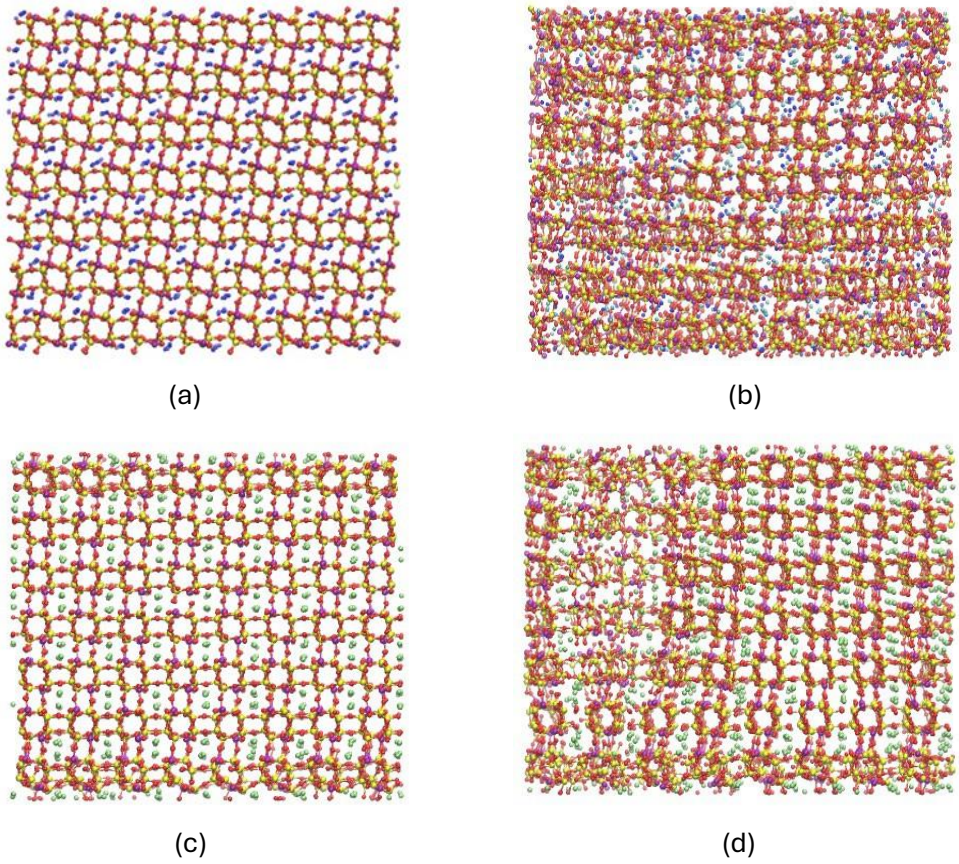

(a) (b)

(c) (d)

Figure 3: (a) structure of forsterite at equilibration (b) structure of forsterite at elongation . (c) structure of magnesite at equilibration. (d) structure of magnesite at elongation.

Chapter 3 – Results and Discussion

3.1. Stress-strain behavior of the forsterite and magnesite.

Multiscale modeling techniques serve as a crucial bridge between atomic-level interactions and macroscopic material behavior, with the investigation of the stress-strain relationship emerging as a particularly dependable method[39]. Through analysis of material properties using microscale models under conditions such as uniaxial tensile or compression tests, researchers gain valuable insights into how materials deform and respond. These properties exhibit notable sensitivity to varying strain rates and temperatures[40]. In atomistic simulations, the concept of continuum Cauchy stress closely corresponds to the definition of Virial stress, both derived from the virial theorem, effectively capturing the forces acting on individual atoms within the system. By computing the per-atom pressure tensor, scientists derive stress values that align with experimental observations, thereby advancing our comprehension of material strength properties and facilitating informed material design for real-world applications[41].

Here, both uniaxial tensile and compression tests have been performed to study and compare the stress-strain results between these two monocrystals for different strain rates and temperatures. Three different temperatures (300K, 500K, and 700K) for a constant strain rate of $0.01ps^{-1}$ and three different strain rates ($0.001ps^{-1}$, $0.01ps^{-1}$, and $0.05ps^{-1}$) for a constant temperature at 300K are considered to make deformation under uniaxial tensile and compression tests. For both minerals, the evolution of the stress values as a function of strain values is studied along the crystallographic direction of [100] in the x direction of the crystals.

3.2. Stress-strain behavior of the geomaterials for different temperatures.

Figure 4a shows a good reference of Young's modulus-based stress-strain curve to study the mechanical properties of the two geomaterials. The curve depicts that the ultimate strength/stress point is the maximum stress for any material before failure occurs under tensile or compression load. The elongation of the elasticity of any material depends on the values of this maximum stress point. Before reaching this point, the loading stress increases with the increasing strain values. However, after the peak point, the material faces deformation and belongs to the plastic region. In this region, the stress values usually decrease with increasing strain values. Now, **Figures 4b and 4c** represent such types of stress-strain relationships of the crystals (forsterite and magnesite, respectively) under a constant tensile load for the temperatures of 300K, 500K, and 700K, at a strain rate of 0.01 ps^{-1}. As expected, a parabolic evolution of the stress values corresponding to the initial linear portion of the stress-strain curves has been observed for both crystals. For forsterite (**Figure 4b**), the ultimate strength point is near 26 GPa at 300K, and Young's modulus value is around 154. 74 GPa, and this value was validated with the result of Young's modulus (153.2 GPa) calculated by Gouriet et al. [28]. Again, at 500K and 700K, the corresponding ultimate strength values are found near 21.79 GPa and 17.92 GPa, respectively. The increasing temperatures from 300K to 500K and 700K initiated a considerable drop in the yield stress of forsterite by 16.15% and 31.07%. More importantly, the increasing temperature also increased the maximum strain values to obtain the maximum stress point. For instance, at 300K, the maximum stress point was achieved for a strain value of 0.168, whereas at 500K and 700K, those maximum points were obtained at the strain values of 0.181 and 0.199, respectively.

From **Figure 4c**, the ultimate strength point for magnesite is found near 13.90 GPa (at 300K) with the corresponding value of Young's modulus at 92.84GPa. This value was validated with the calculated result of Yao et al. [26]. Then, at 500K and 700K, the ultimate strength values are

decreased by 19.42% and 34.46%, respectively. In addition to that, the maximum strain values were decreased by 10.06% (for 500K) and 13.42% (for 700K) from the temperature at 300 K. This incident for magnesite converses to the case of forsterite and indicates that at elevated temperatures, forsterite tends to act as a more elastic material. **Table 5** provides information on Young's modulus values of forsterite and magnesite for different temperatures.

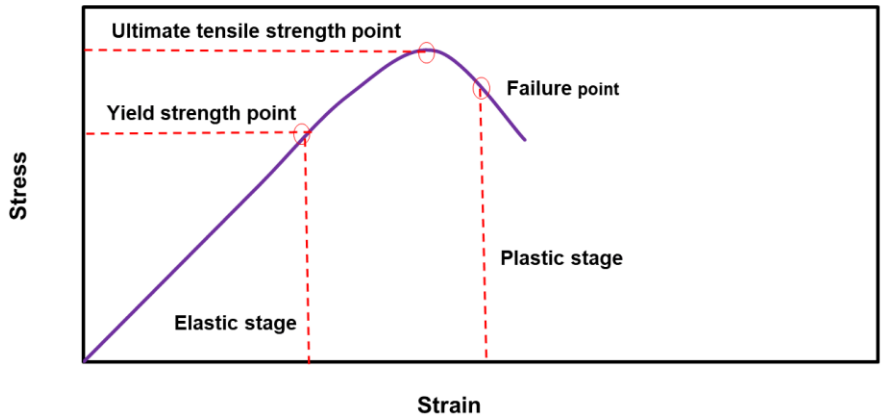

(a)

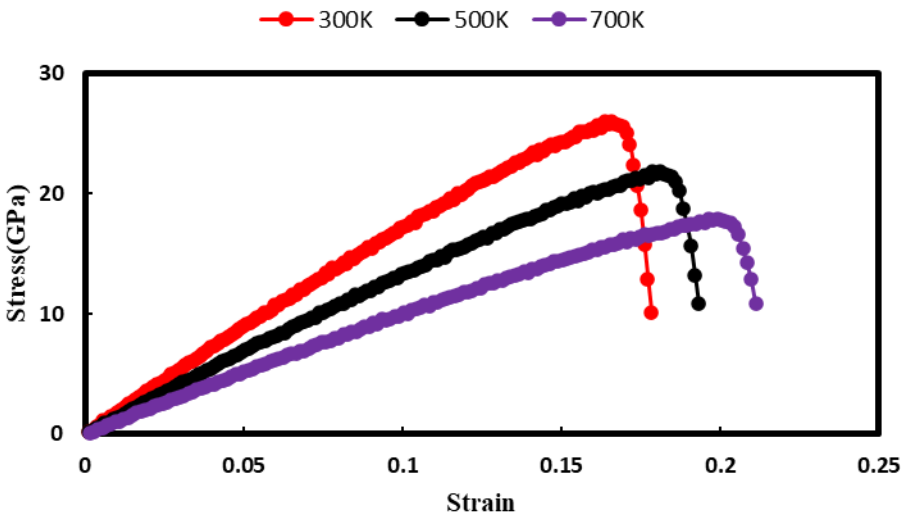

(b)

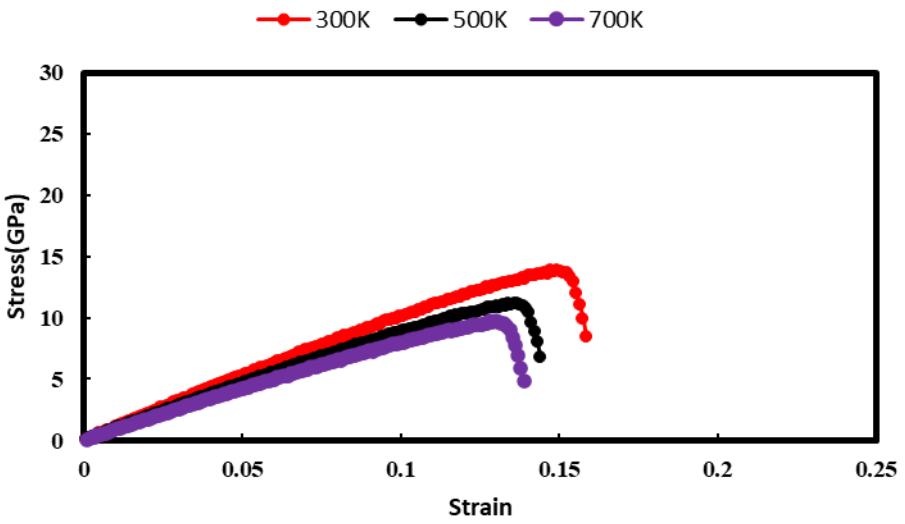

(c)

Figure 4: (a) A generalized physical model of the stress-strain relationship for any material. (b) The stress-strain curve of forsterite for different temperatures under tensile test (at a strain rate of $0.01ps^{-1}$). (c) The stress-strain curve of magnesite for different temperatures under tensile test (at a strain rate of $0.01ps^{-1}$).

Table 5: Ultimate strength and Young's modulus of forsterite and magnesite under tensile and compressive forces.

Material Type	Tensile Force					
	Ultimate Strength (GPa)			Young's Modulus (GPa)		
	Temperature(K)			Temperature(K)		
	300	500	700	300	500	700
Forsterite	26.00	21.80	17.92	154.74	120.79	89.98
Magnesite	13.90	11.20	9.12	92.84	83.58	70.67
Material Type	Compressive Force					
	Ultimate Strength (GPa)			Young's Modulus (GPa)		
	Temperature(K)			Temperature(K)		
	300	500	700	300	500	700
Forsterite	17.28	15.12	13.44	120.45	98.49	77.83
Magnesite	11.08	9.15	7.65	72.96	68.66	62.80

Contrarily**, Figures 5a and 5b** show the stress-strain curves of forsterite and magnesite under the uniaxial compression test, respectively, for the same conditions as for the uniaxial tensile test. The stress-strain relations under this compressive force represent a similar changing process as under tensile force at different temperatures. Since compressive force usually provides more strain

energy to the materials, then the ultimate stress loading stage will be found earlier than the case of tensile force[42]. This increasing strain energy initiates the material to be placed in the plastic stage[40]. For Forsterite (**Figure 5a**), the ultimate stress point is observed at 17.28 GPa at 300K and a strain value of 0.143, where the calculated Young's modulus is about 120.45 GPa. Increasing temperatures to 500K and 700K reduces the maximum stress point near 15.12 GPa and 13.45 GPa, respectively. So, the influence of temperatures on changing stress properties under compressive force is observed similar to tensile force. However, due to the contraction under compressive forces to the crystal material, the elastic stage ended faster than the elongation for tensile force[43]. For example, under compressive stress at 300K, the elastic stage comes to an end at a maximum stress point of 17.28 GPa (**Figure 5a**), whereas, for tensile stress, it reached 26 GPa (**Figure 4b**). In magnesite (**Figure 5b**), the increasing stress loads (up to a strain value of 0.107) couldn't provide any significant change in the elastic stage under compressive force for each temperature (300K, 500K, and 700K). But, after that, the maximum values of the stress load of the magnesite are lower for increasing temperature. This behavior of the crystals under tensile and compressive forces has indicated that increasing temperature (300K) causes more deformation in both crystals. The reason is high temperature contributes more sources of local stress for propagation/stretching out of the crystals [42]. Therefore, the minerals faced more deformation at higher temperatures. However, the results also show that increasing the temperature from 300K to 500K and 700K under compressive force reduces Young's modulus of forsterite (from 120.45GPa to 79.98GPa, respectively) more than magnesite (from 77.04GPa to 60.88GPa, respectively).

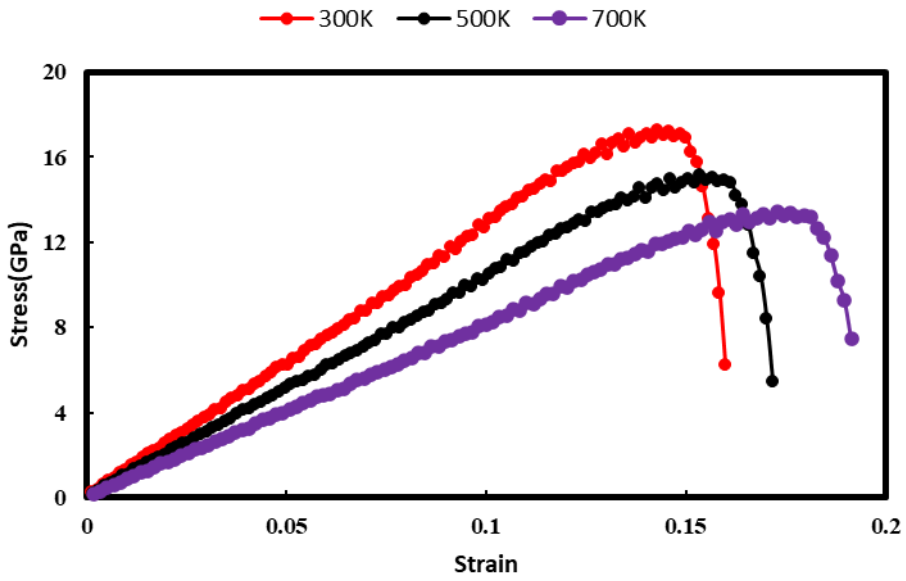
300K
500K
700K
Stress(GPa)
Strain
0
4
8
12
16
20
0
0.05
0.1
0.15
0.2

(a)

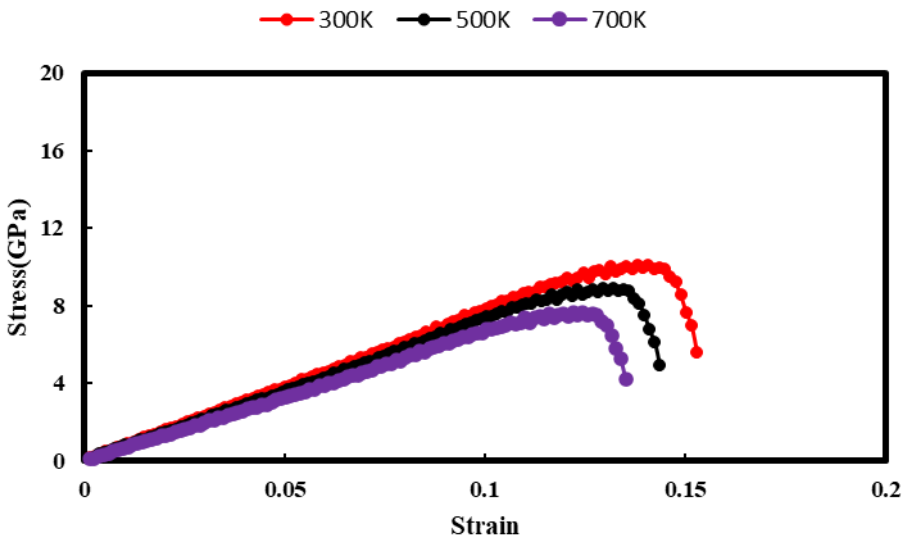
300K
500K
700K
Stress(GPa)
Strain
0
4
8
12
16
20
0
0.05
0.1
0.15
0.2

(b)

Figure 5: (a) The stress-strain curve of forsterite for different temperatures under compression test (at a strain rate of $0.01ps^{-1}$). (b) The stress-strain curve of magnesite for different temperatures under compression test (at a strain rate of $0.01ps^{-1}$).

Therefore, the effects of increasing temperatures are the same for both crystals under two different loading velocities. In both cases, the increasing temperatures provide smaller peaks of stress, but with higher ductility (for forsterite) and lower ductility (for magnesite) up to the failure point of the crystals. Forsterite shows more ductility at elevated temperatures than magnesite. The results obtained from the uniaxial tensile and compressive force for the two crystals at a fixed temperature (600K) are shown in **Figure 6** and given in **Table 6**. Here, in this study, the tensile strength of both minerals is higher than the compressive strength for the applied forces in the [100] crystallographic direction. This was also proved by the previous study done by Gouriet et al. (2019) where the researchers found that the ideal tensile strength (ITS) of forsterite along the (100) crystallographic direction is around 29.3 GPa compared to the ideal compressive strength (ICS) around 12GPa[28]. Therefore, the anisotropic natures of geomaterials vary significantly with their crystal directions.

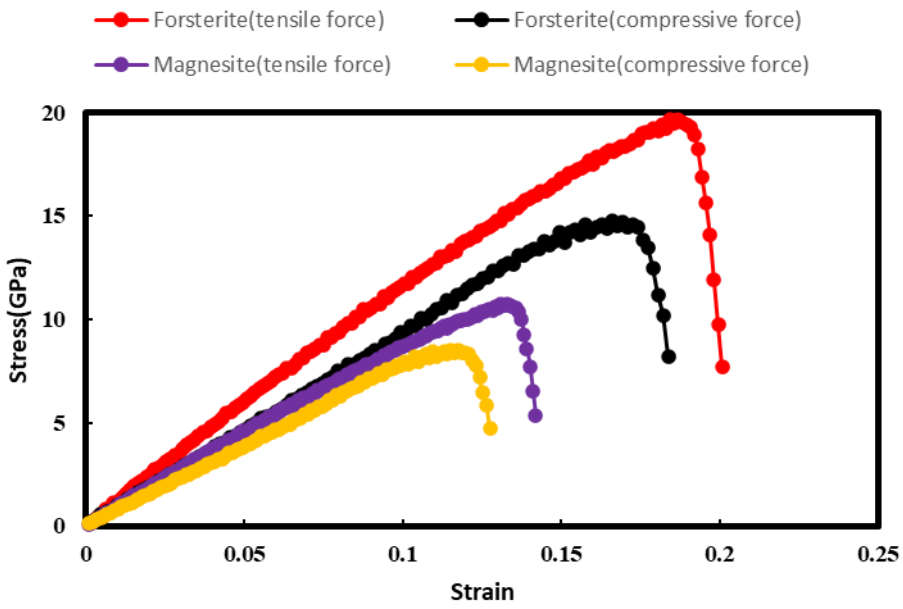

Figure 6: The stress-strain curves for a constant temperature (600K) under different tests.

Table 6: Comparison of the obtained results at 600K for two different applied forces.

Material Type	Maximum Stress Reduction from tensile force to compressive force (%)	Strain variation in achieving maximum stress loading capacity for different applied forces (%)
	Temperature(K)	
	600	600
Forsterite	25.01	11.18
Magnesite	20.12	13.26

In addition, **Figures 7a and 7b** show the evolution of strain energy as a function of strain for a constant temperature (at 600K) to understand the changing of energy during the applied force. The strain energy can be calculated from the potential energy of the system as expressed in equation 4. This strain energy is the difference between the total potential energy and the potential energy of the system in its relaxed, unstrained state. It represents the energy stored in the system due to the applied deformation [40]. From **Figure 7b**, the strain energy of the microstructure (after the relaxation period) changes with strain values. For both crystals, each curve has an inflection point indicating the maximum strain energy the minerals can tolerate. This peak is for the crystals' maximum stress point (ultimate strength). After crossing the peak, the system starts dissipating energy for the deformation in the crystals. The strain energy starts reducing since the loss of energy is higher then. However, similar findings have been noticed in the strain energy curve as well as the stress-strain curve. Forsterite shows higher ductility and elastic properties for both types of applied forces (strain energy ranges from 12.02-15.05 meV/A^3) than magnesite.

$$U_{strain} = U_{total} - U_{relaxed} \quad \ldots\ldots\ldots\ldots\ldots\ldots \quad (4)$$

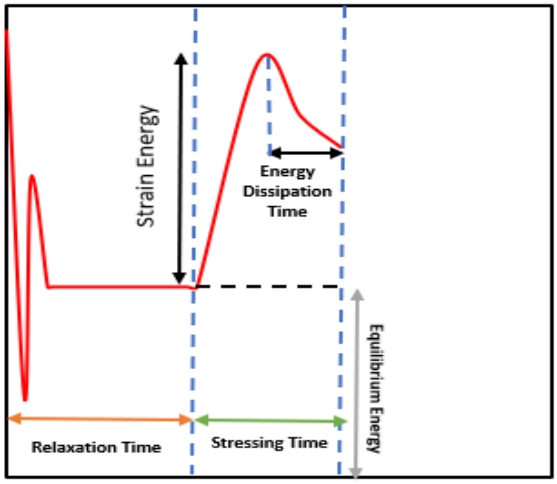

(a)

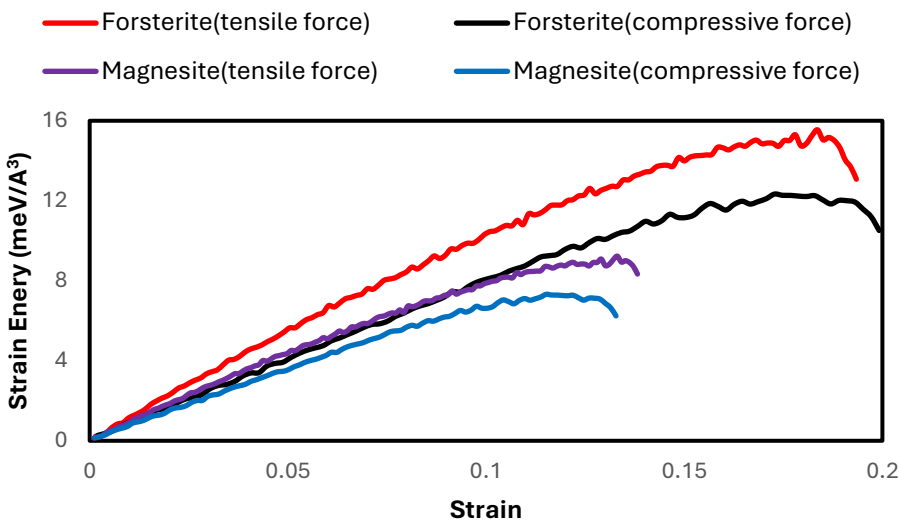

(b)

Figure 7: Evolution of strain energy as a function of strain (a) a generalized curve, (b) for both forsterite and magnesite at 600K.

3.3. Stress-strain behavior of the geomaterials for different strain rates.

In this section, different strain rates are considered to study the impact of loading velocity on the mechanical deformation of both crystals. For this purpose, three different loading rates (0.001,

0.01, and 0.05 ps^{-1}) are applied under both tensile and compressive forces. The effect of different loading rates has been studied previously on different crystals using molecular dynamics simulation. It should be noted that the crystals were in a relaxation state before applying both tensile and compressive forces. That's why the stress values as a function of strain values are started from the undeformed state of the crystal (at a strain value of zero) either for increasing or decreasing loading velocities. Generally, **Figures 8a and 8b** show the stress-strain curves for forsterite and magnesite at a constant temperature of 300K (under tensile force), respectively, for the three abovementioned loading rates. According to the results demonstrated in the figures, the increasing strain rates increase the maximum yield points for both crystals. Particularly, the increasing strain rates have exceeded the elastic stage, but have no impact on the plastic stage. The yield points are just changed for different loading velocities. In addition, the strength of non-viscoelastic materials like crystals greatly depends on the different loading rates; a higher strain rate indicates a higher strength of the material. For forsterite (**Figure 8a**), the increasing strain rate from 0.01 ps^{-1} to 0.05ps^{-1} increases the maximum stress point by 10.71% and the decreasing strain rate to 0.001ps^{-1} decreases the 11.43%. In the case of magnesite (**Figure 8b**), the maximum stress point moves to 15.21GPa for the loading rate of 0.05ps^{-1}, whereas the peak stress point is decreased by 18.30% for the decreasing strain rate to 0.001ps^{-1}. Under applying compressive force, the changes in the stress-strain relationship follow a similar trend for both materials like the tensile force. **Figure 9a** shows the results for forsterite, whereas the changes for magnesite are shown in **Figure 9b**.

Here, for higher strain rates, the values of strain energy increase for both forsterite and magnesite to initiate plastic deformation. This is contradictory to the case of higher temperatures. The higher strain rate provides a smoother trend of the stress-strain relationship (more linear) reason for

having a shorter time to break during deformation. This higher strain rate makes the elastic region more linear, which is considered Hooke's law. This required energy is higher for tensile force than compressive force. Hence, the forsterite shows more strength at a higher strain rate compared to the magnesite. The results of the stress-strain relationship between these two crystals obtained under both forces are compared for a constant strain rate (at 300K and a strain rate of $0.03ps^{-1}$), and those results are shown in **Figure 10**. This specific strain rate is considered here to show the changes and compare the stress-strain relationship evolution for both minerals under tensile and compressive forces.

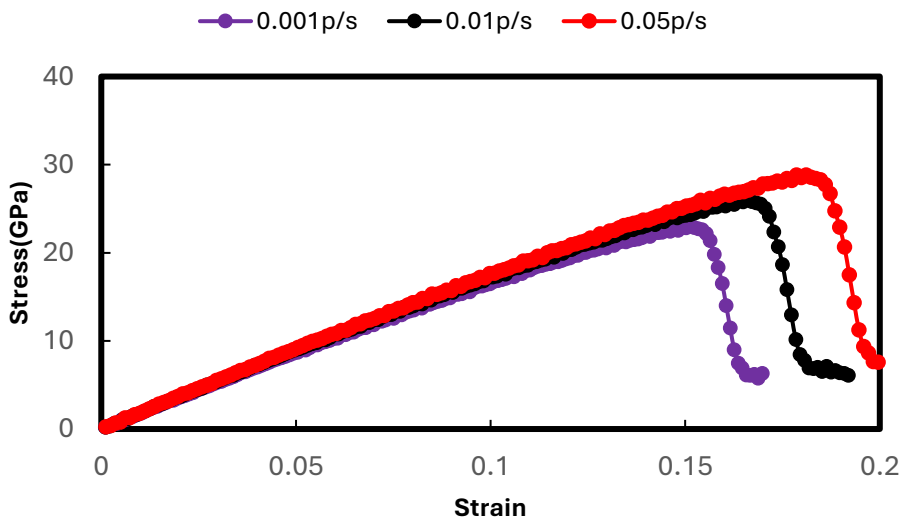

(a)

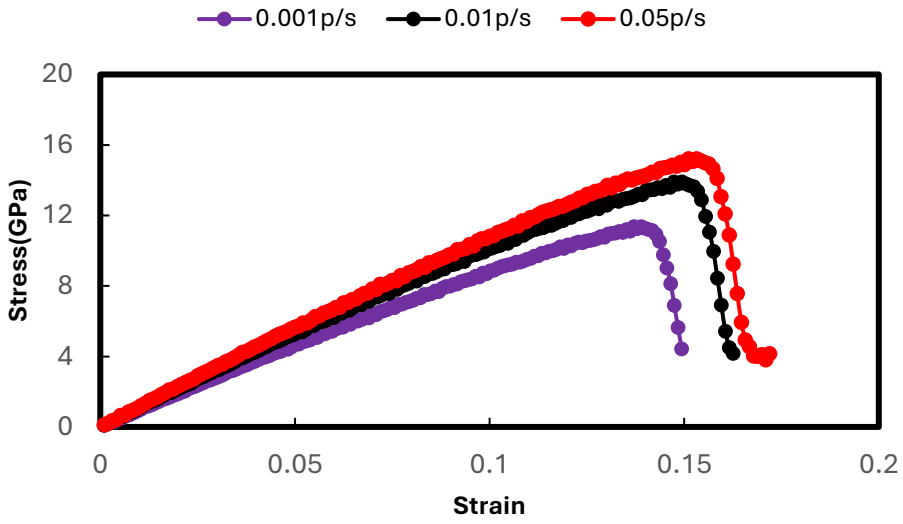

(b)

Figure 8: (a) The stress-strain curve of forsterite for different strain rates under tensile test (at 300K). (b) The stress-strain curve of magnesite for different strain rates under tensile test (at 300K).

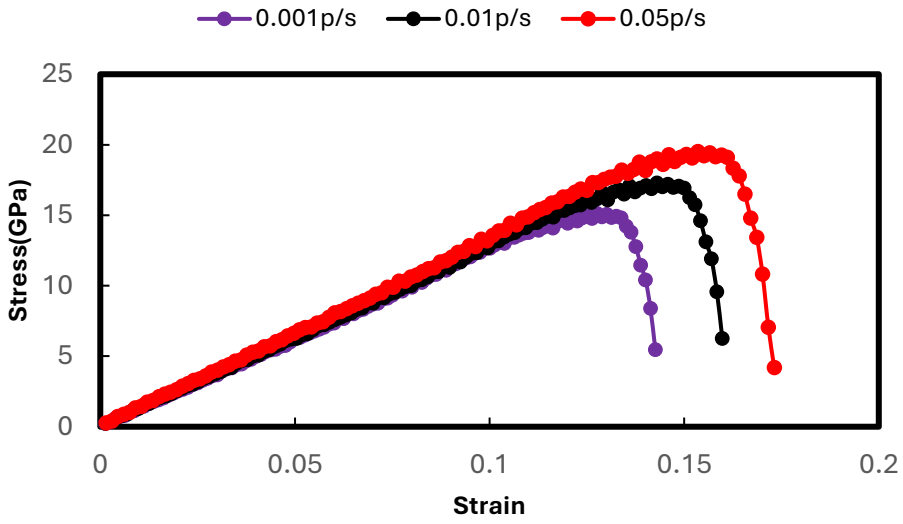

(a)

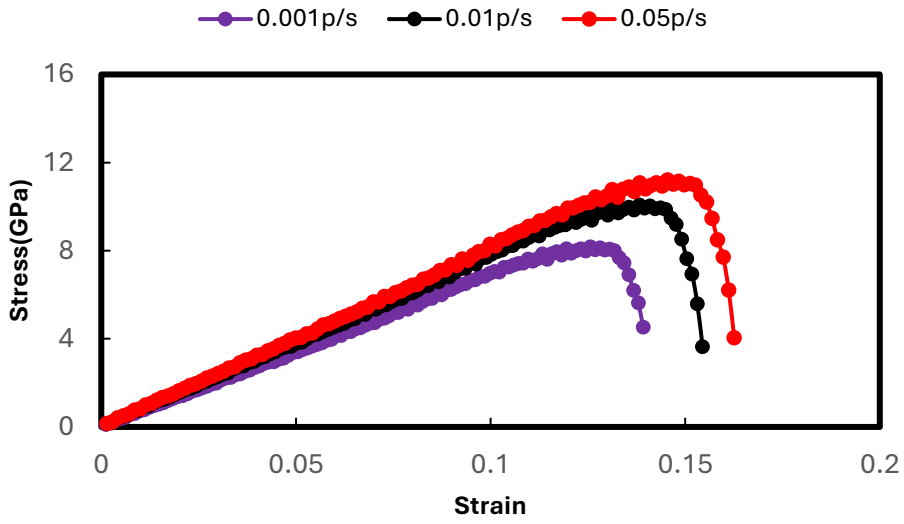

(b)

Figure 9: (a) The stress-strain curve of forsterite for different strain rates under compression test (at 300K). (b) The stress-strain curve of magnesite for different strain rates under compression test (at 300K).

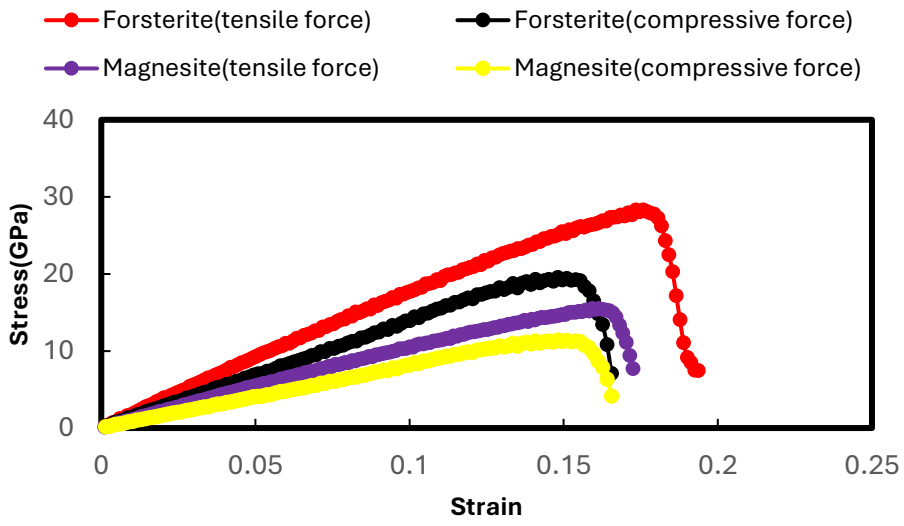

Figure 10: The stress-strain curves for a constant strain rate ($0.01ps^{-1}$) under different tests.

3.4. Strain Rate Sensitivity

The strain rate sensitivity (SRS) measures the change in yield pressure for different strain rates of material. Sometimes, applied force alters the characteristics of the material which can be understood by SRS calculation. This is a relationship where a material's tensile strength depends on different loading rates. Based on the conditions of a steady state process, the SRS of a material in loaded tension can be demonstrated (as a differential form) by Hart [44] as follows:

$$m = \frac{\partial \log \left({}^{\sigma_2}/_{\sigma_1} \right)}{\partial \log \left({}^{\acute{\varepsilon}_2}/_{\acute{\varepsilon}_1} \right)} \quad \text{.....(5)}$$

Where, m=strain rate sensitivity (unitless), σ_1, and σ_2 = tensile strength, and $\acute{\varepsilon}_1$ and $\acute{\varepsilon}_2$ = strain rate.

Hence, equation (4) states that the SRS values can be obtained from the slopes of the logarithmic plot of tensile stresses and corresponding strain rates. Hart [44] exhibited that stress rates are proportional to strain rates up to the ultimate/maximum strength point. The influence of SRS is observed normally as an increase in yield strength (the limiting value of the stress) of the material. Because, after the beginning of the plastic deformation, the material is less sensitive to the extra load. Therefore, for higher strain rates, the SRS is found higher. On the contrary, higher temperatures reduce the SRS of material for the corresponding strain rates. The higher the values of SRS are, the lower the strength of the materials would be. This relationship of SRS with different strain rates and temperatures is not similar.

Simulations were performed for three different temperatures (300K, 500K, and 700K) and three different strain rates ($0.001ps^{-1}$, $0.01ps^{-1}$, and $0.05ps^{-1}$) to determine and compare the obtained SRS results between forsterite and magnesite. Here, steady strain rate sensitivity is considered, where the strain rate sensitivity coefficient, m is computed using the above-mentioned equations using the corresponding strain rates. The obtained SRS values here are found negative, indicating the

conditions of the stability of the materials. **Figures 11(a) and 11(b)** show the variations of m values with strain rates for forsterite and magnesite, respectively for different temperatures and strain rates. For forsterite and magnesite (**Figures 11a and 11b**), at a constant strain rate ($0.01ps^{-1}$), the increasing temperatures from 300K→500K→700K enhance the m value from -0.70→-0.66→-0.62 and -0.57→-0.52→-0.47. Both forsterite and magnesite become less stable at higher temperatures. On the other hand, for a constant temperature (300K), when the strain rates jump from $0.001ps^{-1}$→$0.01ps^{-1}$→$0.05ps^{-1}$, then the m values decrease from -0.45→-0.70→-1.11 and -0.36→-0.57→-0.90, for forsterite and magnesite, respectively. Hence, both materials show less sensitivity to increasing strain and more stability for higher strain rates. On the other hand, for a constant temperature (300K), when the strain rates jump from $0.001ps^{-1}$→$0.01ps^{-1}$→$0.05ps^{-1}$, then the m values decrease from -0.45→-0.70→-1.11 and -0.36→-0.57→-0.90, for forsterite and magnesite, respectively. Hence, both materials show less sensitivity to increasing strain and more stability for higher strain rates. So, higher temperatures increase the sensitivity of materials to strain rate and decrease the yield strength.

Now, from the above results, it has been found that forsterite shows less sensitivity than magnesite, which means that magnesite is comparatively less stable at higher temperatures. The comparison of the results for both crystals is shown in **Figure 12**. At a constant temperature (500K), the SRS values of forsterite and magnesite are -0.43 and -0.32, -0.66 and -0.52, and -1.04 and -0.86 for the strain rates of $0.001ps^{-1}$, $0.01ps^{-1}$ and $0.05ps^{-1}$, respectively. However, despite having a lower strain effect at lower temperatures, the influence of temperatures on SRS is observed significantly higher for lower strain rates. Because the sensitivity arises from the inertness of defective structure evolution of material for lower strain rates [40]. Since the strength of the materials is disproportionate to the SRS, both crystals are prompted to deform earlier when the SRS values are

higher for corresponding temperatures and strain rates. The impact of temperature is found higher in tensile strength for magnesite than forsterite which agrees with the stress-strain curves in the previous section. So, higher sensitivity to applied forces makes the magnesite less strong material than forsterite.

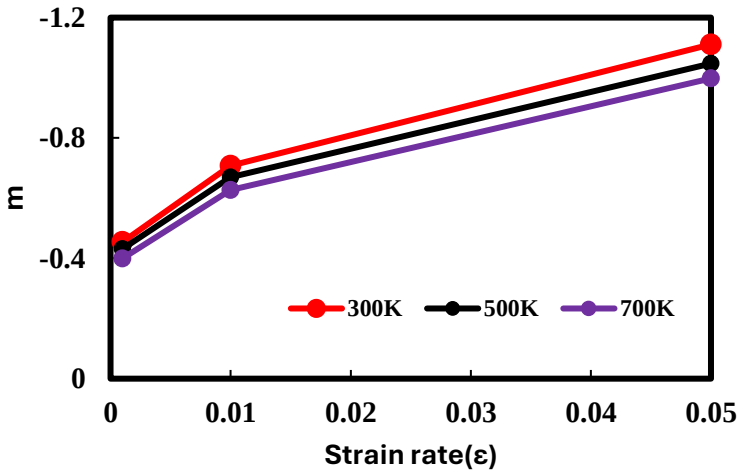

(a)

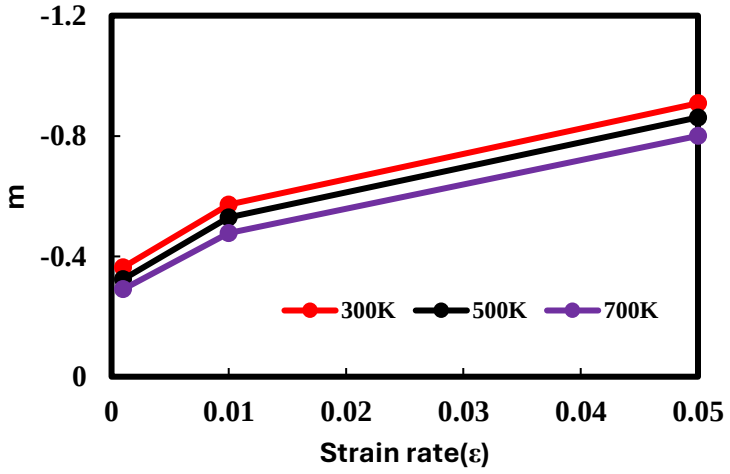

(b)

Figure 11: Strain rate sensitivity of (a) forsterite and (b) magnesite, for different temperatures (300K, 500K, and 700K) and strain rates ($0.001ps^{-1}$, $0.01ps^{-1}$, and $0.05ps^{-1}$).

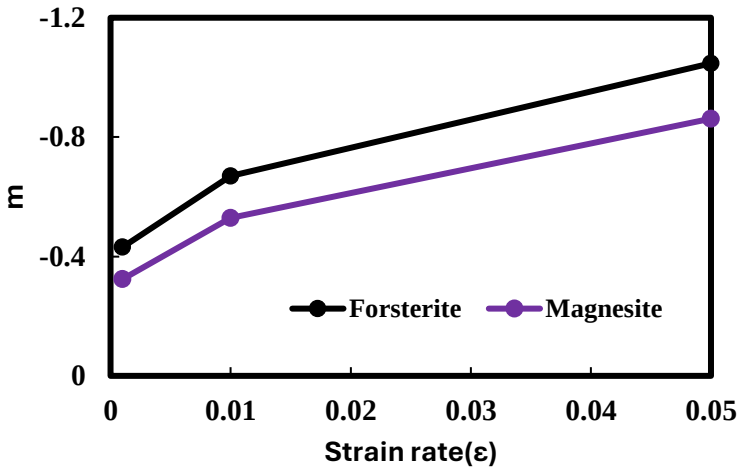

Figure 12: Strain rate sensitivity of both forsterite and magnesite at 500K.

3.5. Effect of grain size

The impact of grain size on both crystals is studied here. Crystals are comprised of multiple grains, and these grains are bounded by some interfacial defects in the grain boundaries of those crystals. These grains' structure and energy provide microscopic insight into the mechanical deformation of the polycrystals. Particularly, the morphology, size distribution, and nature of these grains and grain boundaries are important features of those crystals [45]. Also, the grain size and boundaries resist the elongation of those crystals and reduce the yield strength and ductility of the materials. However, there is a significant correlation between grain size and mechanical strength properties of the mineral (particularly on sedimentary rocks) which has been proved by previous studies [46]. The study on grain size microstructure provides insights into the materials' toughness, corrosion resistance, thermal conductivity, and magnetic susceptibility.

Hence, the compressive strengths of the two crystals are evaluated physically for decreasing grain sizes. Ajalloeian et al. [47] found a generalized relationship between the compressive strength of

the materials and the grain size of the materials and stated that there is a growing trend of mechanical strength for increasing grain size. Also, Meng and Pan [48] investigated the petrophysical and mechanical properties of carbonate minerals for different grain sizes and claimed that the decreasing of average grain sizes reduces the strength properties of the materials. Since there is a relationship (nonproportional) between grain size and density of the materials, hence in this study, the atoms numbers are increased for both minerals to study the impact of grain size [49]. Because the more the number of atoms will be closely packed, the higher the density of the materials would be with smaller grain sizes.

Figure 13 shows the yield strengths of both forsterite and magnesite at a constant strain rate ($0.01ps^{-1}$) for 5600 atoms and 4850 atoms, respectively, as well as comparing those with previous systems. This figure shows that crystals are more deformative for growing atom numbers. The yield strengths of the forsterite and magnesite dropped by 7.89% and 9.09% than the initial systems. These results show an opposite correlation between compressive strength with atom numbers. From the figure, it has been observed that the grain size also impacts Young's modulus of the two crystals (dropped at 15.92 and 9.17 GPa, respectively). In the case of these two crystals, the components only bearing the applied stress are grains. In addition, the distribution of the grains becomes uniform for higher atom numbers, hence the deformation of the crystals happened earlier from the pristine conditions of the low number of atoms. However, shear velocity, wave velocity, relatively low energy, and partial double-bond character in Si-O and C-O bonds also cause the reduction in strength properties for lower grain sizes. However, these discussions are not part of our current study.

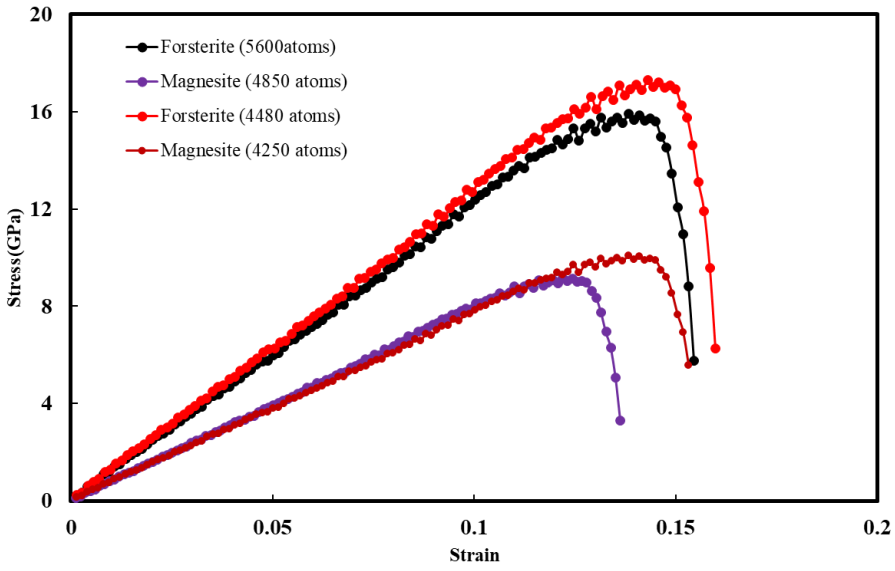

Figure 13: Compressive strength curve of forsterite and magnesite for different grain sizes.

3.6. Elastic Properties

Elastic properties are crucial parameters of the earth's minerals to be utilized in geophysics and geochemistry to understand and explain the interior information of the earth. These properties are indispensable for characterizing the rheology of geotectonic and constructing the seismic acoustic waves in solid-state physics. The elastic properties represent the ability of the materials to deform for a small change in stress. The crystal structure, composition, and microstructure of any material could be illustrated from these properties. Based on these properties, the compositional change, as well as the elongations in the material, can be observed.

The elastic constant is the ratio of the second derivative of energy density concerning the strain and simply can be expressed as in equation (6) [50].

$$C_{ij} = \frac{1}{V}\frac{\partial^2 E}{\partial \varepsilon_i \partial \varepsilon_j} \quad \text{.....(6)}$$

Where, C_{ij}= component for stiffness coefficient, V= volume of the unit cell, E= energy, and ε= strain.

Here, for calculating the elastic constants, a three-dimensional fourth-order Voigt notion model was used which generally considers the basis of Hooke's law, finite element analysis, and diffusion MRI[50]. This model is convenient for providing elastic constants of a material as a 6*6 matrix. But, hence, only three pressure and temperature-dependent elastic stiffness constants (C_{11}, $C_{33,}$ and C_{44}) for both forsterite and magnesite crystals have been considered to study the mechanical deformation of the minerals. These elastic constants could also provide information about the materials' bulk modulus and shear modulus, but those are not part of this study.

Figures 14 and 15 show the pressure and temperature-dependent elastic constants for both forsterite and magnesite crystals. The obtained results agree well with the previous works. For both forsterite and magnesite, the elastic constant values of C_{11}, $C_{33,}$ and C_{44} at zero-point motion and 300K (known as static conditions) were validated with previous work [49], [26]. From Figures 14 and 15, the pressure and temperature changes noticeably affect the elastic constants of those two crystals. For forsterite (Figure 14a), the changes in pressure from 0GPa to 100GPa increased the values of C_{11}, $C_{33,}$ and C_{44} to 344.73, 620.59, and 859.89GPa, respectively. On the other hand, these values were found near 220.61, 347.25, and 462.89GPa respectively for magnesite (Figure 15a). So, it can be observed that the elasticity is linearly dependent on the applied pressure. Because at higher pressures, both forsterite and magnesite undergo a phase transition to a denser crystal structure. Also, Young's modulus values for these minerals are higher. Besides, the higher pressure changes the bonding between the atoms. These phenomena cause the elastic properties of the minerals to be higher. Hence, the higher pressure and elasticity results in higher tensile strength for the two minerals.

On the contrary, the increasing temperature increases the atomic vibration through the crystal structure and continues to reach the value where the atomic bonds become weak [26]. This causes

disorder and irregularity in the crystal lattice. As a result, the elastic properties of the minerals decrease, and the minerals become less resistant to deformation. Hence, the temperature increased from 300K to 700K decreased the values of C_{11}, C_{33}, and C_{44} for forsterite by 35.94%, 45.33%, and 49.10% (Figure 14b), and for magnesite by 41.98%, 30.76%, and 47.09% (Figure 15b), respectively. Consequently, the temperature change has a non-proportional relationship with the elasticity of the materials. Because, at the higher temperature, the materials must go through higher thermal vibration which increases thermal expansion inside the materials but reduces the tensile strength and corresponding lattice constants. For this reason, two crystals showed lower elasticity at increasing temperatures. The study of these elastic properties for different pressures and temperatures is essential for investigating the phase transition of minerals (including mineralogy or geology). This phase transition is very helpful in interpreting the geophysical data and design of those minerals for their desired properties. Again, this study can give insights into developing the model of those minerals for predicting behaviors under extreme conditions.

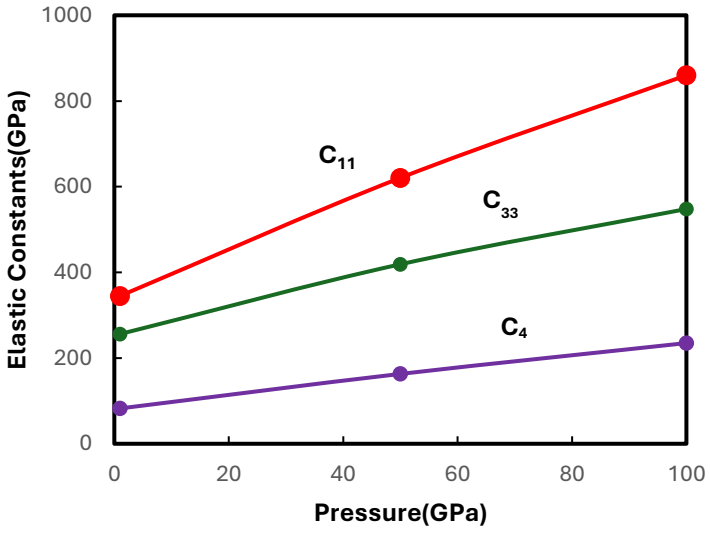

(a)

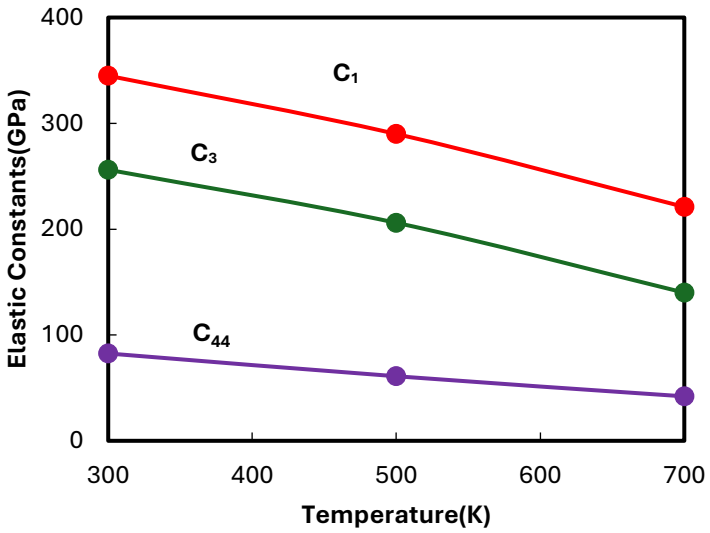

(b)

Figure 14: Elastic constants of forsterite, (a) effect of pressure, and (b) effect of temperature.

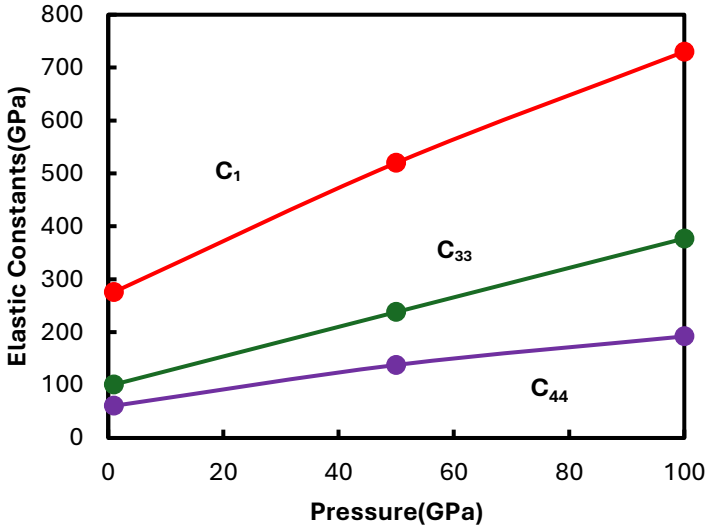

(a)

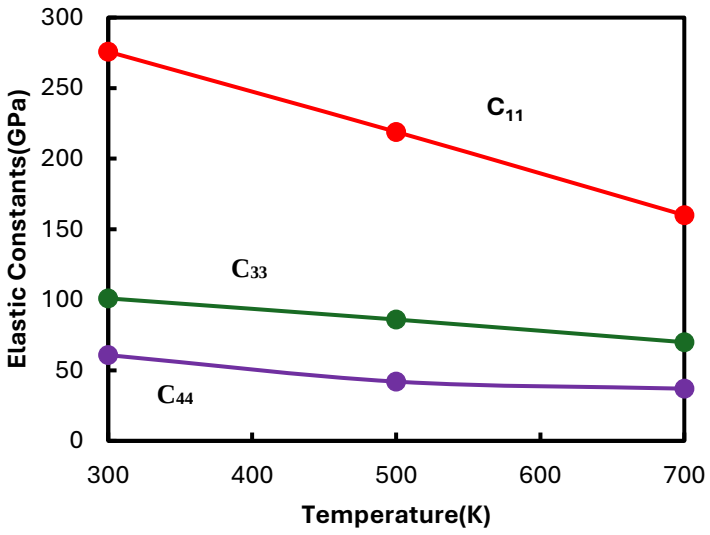

(b)

Figure 15: Elastic constants of magnesite, (a) effect of pressure, and (b) effect of temperature.

3.7. Radial Distribution Function

The radial distribution function (RDF) on any bonded simulated system is calculated mainly to determine the pairwise interaction and coordination number between the groups of nearest neighbor atoms[52][53]. Here, it measures the probability of finding a particle at a specific distance (r) from a reference particle in the mineral. Particularly, this function determines the distribution of neighboring particles around a center particle. The RDF for any bonded system can be expressed as follows:

$$g(r) = \frac{\rho(r)}{\rho} \quad \text{.....(7)}$$

Where, ρ(r)= the average local number density of particles at a distance r, and ρ= the bulk density of the particles.

The histogram form represents the RDFs calculation by binding the pairwise interaction into several bins distance. This distance is specified as the pair cutoff distance (r) for a particular

potential field. This RDF is counted only for the specified cutoff distance, and the coordination of any atoms beyond this distance is out of consideration. This RDF function shows better results (with multiple peaks in the histogram) if the system is uniform and well-equilibrated. Otherwise, if the system is not either uniform or well-equilibrated, there will be a sharp change in the coordination of the atoms with one single peak due to less interaction.

Here, **Figure 16** shows the pair RDFs for both disordered structures of forsterite and magnesite crystals. Only the pairwise interactions between Si-O and C-O atoms are considered for this RDF calculation since the bonded interactions of those atoms are the most contributing factors for providing strength in the respective crystals. Even though several peaks can be seen in the figure, only the sharp peak is considered the strongest interaction between the pair atoms. The red curve is obtained from the Si-O atoms whereas C-O provides the black one. These two RDF curves are obtained from the trajectories of the coordination numbers of their bonded atoms. The highest peak of the first curve is found around 2.54 angstrom which indicates the strongest interaction between the bonded Si-O atoms. On the other hand, this highest peak position is seen at 3.26 angstrom for C-O bonded atoms. In addition, the densities of both bonded Si-O and C-O atoms are higher in those peak points of the curves. These two curves' peak intensity indicates that the oxygen atoms usually attract the Si atoms more strongly than the C atoms. However, from the calculation RDF for these two crystals, it has been observed that the less interaction between the carbon and oxygen atoms than the silicon and oxygen atoms make the magnesite mineral less strong material from the forsterite minerals.

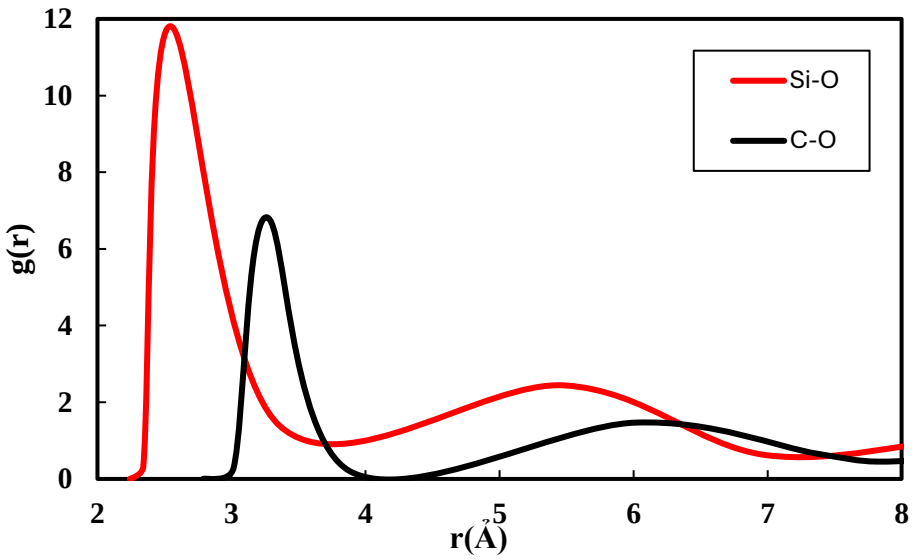

Figure 16: Pairwise Radial Distribution Function of forsterite and magnesite samples.

Chapter 4- Conclusions and Future Work

At the microscale, the presence of many mineral phases as well as microstructural defects distinguishes geomaterials, which are known to be multiscale heterogeneous, and discontinuous. In summary, this study examines the changes in mechanical properties between the forsterite and magnesite crystals using molecular dynamics simulation for different conditions. A direct comparison can be made between each computation as the MD simulation allows for the splitting of energy data calculation into individual parts such as surface energy, elastic energy, and plastic energy. In this work, the effects of strain rate and temperature on the stress-strain properties are studied on crystal models.

The significant findings of this research are listed below:

- The Young's modulus of forsterite and magnetite are found near 154.74GPa and 92.84GPa under tensile force. These values are found around 120.45GPa (forsterite) and 77.04GPa (magnesite) for compressive force. The increasing temperature reduces the maximum strength of the crystals. For higher temperatures, forsterite shows higher ductility than magnesite.
- Higher strain rates require higher strain energy to initiate plastic deformation in the crystals. This phenomenon is opposite to the case of increasing temperature, whereas the increasing temperature requires lower energy for initiating plastic deformation.
- According to the strain rate sensitivity results, magnesite shows less sensitivity to applied force than forsterite. At, 300K and a strain rate of $0.01ps^{-1}$, the SRS values of forsterite and magnesite are found near -0.70 and -0.57, respectively. The results also state that the impact of temperatures on SRS is higher for lower strain rates.

- Decreasing grain sizes (or increasing atom numbers) reduces the mechanical strength properties of the crystals. The yield strengths of the forsterite and magnesite dropped by 7.89% and 9.09% than the initial systems.
- The increasing pressure induces phase transition and increases the elastic properties in the crystals. On the other hand, increasing the temperature increases the atomic vibration through the crystal structure and this causes disorder and irregularity in the crystal lattice.
- In addition, from the RDF results, it has been observed that the peak intensity of pairwise interaction between Si-O is higher than the Mg-O.

Finally, this study has found that magnesite is favorable for the comminution process which is the product of mineral carbonation on forsterite. Magnesite shows less ductility at higher temperatures compared to forsterite. The reason behind that is that magnesite faces much more disorder and irregularity in crystal structure than forsterite at increasing temperatures. Contrary, the impacts of pressure and temperature are not the same. The pressure increases the stiffness and hardness of both crystals, while temperature does the opposite. So, it can be said that mineral carbonation impacts the energy requirement of the minerals for the comminution process and this study is considered supportive of the process optimization and energy-saving approaches of mineral processing.

In terms of energy requirement, previous work found that the breaking down of forsterite minerals typically requires a substantial energy input, often around 260kWh per ton of material processed. Contrary, the magnesite mineral demands less energy, typically around 80kWh per ton. Then, the mineral carbonation process involves an energy consumption of 210kWh per ton of forsterite. However, this carbonation process is an exothermic reaction process that usually releases an energy of around 45kWh including achieving 60% CO_2 sequestration efficiency[54].

This simulation study at the microscale level can be applied to the field scale level by considering the heterogeneity, defects, and boundary conditions that can provide information about capturing the challenges. The discussion about the phenomena of changes in the physical properties of minerals can also relate to the complexity and ability to accurately model for larger-scale implications. For example, the bulk properties may differ from those calculations by atomic scale due to the presence of grain boundaries, dislocations, and other defects. Besides, transport properties like diffusion and reaction kinetics can be included which are overlooked here, and can be investigated for larger scale application of this work.

Also, this study can be improved by furthering the initial exploration of material defects, focusing primarily on cracks, dislocations, and shear bonds. Cracks induce stress concentrations within materials, thereby affecting their mechanical properties. Additionally, porosity represents a significant parameter influenced by environmental factors such as temperature and pressure. Porosity not only diminishes material strength but is also intricately tied to pore size, shape, and spatial distribution. It is hypothesized that elevated temperatures can alter the porosity of geomaterials, consequently impacting tensile strength outcomes.

References

[1] F. Wang and D. Dreisinger, “Carbon mineralization with concurrent critical metal recovery from olivine,” *Proc Natl Acad Sci U S A*, vol. 119, no. 32, 2022, doi: 10.1073/pnas.2203937119.

[2] C. D. Hills, N. Tripathi, and P. J. Carey, “Mineralization Technology for Carbon Capture, Utilization, and Storage,” 2020. doi: 10.3389/fenrg.2020.00142.

[3] G. Gadikota, “Carbon mineralization pathways for carbon capture, storage and utilization,” 2021. doi: 10.1038/s42004-021-00461-x.

[4] S. P. Veetil and M. Hitch, “Recent developments and challenges of aqueous mineral carbonation: a review,” 2020. doi: 10.1007/s13762-020-02776-z.

[5] B. Hasanah, “Studi Tingkat Kerusakan Bangunan Rumah Terhadap Serangan Rayap Di Kecamatan Bankit Kabupaten Way Kanan,” *Fakultas Tarbiyah Dan Keguruan IAIN Raden Intan Lampung*, 2021.

[6] P. Renforth, C. L. Washbourne, J. Taylder, and D. A. C. Manning, “Silicate production and availability for mineral carbonation,” *Environ Sci Technol*, vol. 45, no. 6, 2011, doi: 10.1021/es103241w.

[7] E. Bali, N. Bolfan-Casanova, and K. T. Koga, “Pressure and temperature dependence of H solubility in forsterite: An implication to water activity in the Earth interior,” *Earth Planet Sci Lett*, vol. 268, no. 3–4, 2008, doi: 10.1016/j.epsl.2008.01.035.

[8] J. M. Matter and P. B. Kelemen, “Permanent storage of carbon dioxide in geological reservoirs by mineral carbonation,” *Nat Geosci*, vol. 2, no. 12, 2009, doi: 10.1038/ngeo683.

[9] W. J. J. Huijgen and C. R.N.J., “Carbon dioxide sequestration by mineral carbonation Literature Review W.J.J.,” *Energy research Centre of the Netherlands*, vol. ECN-C--03-, no. February, 2003.

[10] T. Xu, J. A. Apps, and K. Pruess, “Analysis of mineral trapping for CO2 disposal in deep aquifers,” 2001.

[11] M. Isshiki *et al.*, “Stability of magnesite and its high-pressure form in the lowermost mantle,” *Nature*, vol. 427, no. 6969, 2004, doi: 10.1038/nature02181.

[12] M. Mazzotti *et al.*, “IPCC Special Report on Carbon dioxide Capture and Storage, Mineral carbonation and industrial uses of carbon dioxide,” *Ipcc*, 2005.

[13] S. Snæbjörnsdóttir, B. Sigfússon, C. Marieni, D. Goldberg, S. R. Gislason, and E. H. Oelkers, “Carbon dioxide storage through mineral carbonation,” 2020. doi: 10.1038/s43017-019-0011-8.

[14] P. B. Kelemen and J. Matter, “In situ carbonation of peridotite for CO2 storage,” *Proc Natl Acad Sci U S A*, vol. 105, no. 45, 2008, doi: 10.1073/pnas.0805794105.

[15] V. Romanov, Y. Soong, C. Carney, G. E. Rush, B. Nielsen, and W. O'Connor, "Mineralization of Carbon Dioxide: A Literature Review," 2015. doi: 10.1002/cben.201500002.

[16] S. Gerdemann, D. Dahlin, and W. O'Connor, "Ex-situ and in-situ mineral carbonation as a means to sequester carbon dioxide," *Osti.Gov*, 2004.

[17] S. J. Gerdemann, W. K. O'Connor, D. C. Dahlin, L. R. Penner, and H. Rush, "Ex situ aqueous mineral carbonation," *Environ Sci Technol*, vol. 41, no. 7, 2007, doi: 10.1021/es0619253.

[18] M. J. Abdolhosseini Qomi, Q. R. S. Miller, S. Zare, H. T. Schaef, J. P. Kaszuba, and K. M. Rosso, "Molecular-scale mechanisms of CO2 mineralization in nanoscale interfacial water films," 2022. doi: 10.1038/s41570-022-00418-1.

[19] P. B. Kelemen, N. McQueen, J. Wilcox, P. Renforth, G. Dipple, and A. P. Vankeuren, "Engineered carbon mineralization in ultramafic rocks for CO2 removal from air: Review and new insights," *Chem Geol*, vol. 550, 2020, doi: 10.1016/j.chemgeo.2020.119628.

[20] D. Tromans, "Mineral comminution: Energy efficiency considerations," *Miner Eng*, vol. 21, no. 8, 2008, doi: 10.1016/j.mineng.2007.12.003.

[21] P. Semsari Parapari, M. Parian, and J. Rosenkranz, "Breakage process of mineral processing comminution machines – An approach to liberation," *Advanced Powder Technology*, vol. 31, no. 9, 2020, doi: 10.1016/j.apt.2020.08.005.

[22] R. P. King, "Comminution and liberation of minerals," *Miner Eng*, vol. 7, no. 2–3, 1994, doi: 10.1016/0892-6875(94)90059-0.

[23] F. Molaei, A. Hamed Mashhadzadeh, C. Spitas, and M. Reza Saeb, "Atomistic analysis of 3D fracture fingerprints of mono- and bi-crystalline diamond and gold nanostructures," *Eng Fract Mech*, vol. 263, 2022, doi: 10.1016/j.engfracmech.2022.108291.

[24] C. W. Holyoke, A. K. Kronenberg, J. Newman, and C. Ulrich, "Rheology of magnesite," *J Geophys Res Solid Earth*, vol. 119, no. 8, 2014, doi: 10.1002/2013JB010541.

[25] Z. J. Liu, X. W. Sun, T. Song, Y. Guo, C. R. Zhang, and Z. R. Zhang, "Atomistic simulation of the structural and elastic properties of magnesite," *Bulletin of Materials Science*, vol. 39, no. 5, 2016, doi: 10.1007/s12034-016-1246-3.

[26] C. Yao, Z. Wu, F. Zou, and W. Sun, "Thermodynamic and Elastic Properties of Magnesite at Mantle Conditions: First-Principles Calculations," *Geochemistry, Geophysics, Geosystems*, vol. 19, no. 8, 2018, doi: 10.1029/2017GC007396.

[27] J. Á. Martínez-González, J. Navarro-Ruiz, and A. Rimola, "Multiscale computational simulation of amorphous silicates' structural, dielectric, and vibrational spectroscopic properties," *Minerals*, vol. 8, no. 8, 2018, doi: 10.3390/min8080353.

[28] K. Gouriet, P. Carrez, and P. Cordier, "Ultimate mechanical properties of forsterite," *Minerals*, vol. 9, no. 12, 2019, doi: 10.3390/min9120787.

[29] R. Choudhary *et al.*, “Impact of forsterite addition on mechanical and biological properties of composites,” *Journal of Asian Ceramic Societies*, vol. 8, no. 4, 2020, doi: 10.1080/21870764.2020.1807695.

[30] J. M. Goodfellow and M. A. Williams, “Molecular dynamics. Current Opinion in Structural Biology 1992, 2:211-216,” *Curr Opin Struct Biol*, vol. 2, no. 2, 1992, doi: 10.1016/0959-440X(92)90148-Z.

[31] A. Fadavi Firooz, A. Hashemi, G. Zargar, and Y. Tamsilian, “Molecular dynamics modeling and simulation of silicon dioxide-low salinity water nanofluid for enhanced oil recovery,” *J Mol Liq*, vol. 339, 2021, doi: 10.1016/j.molliq.2021.116834.

[32] A. G. Newton and G. Sposito, “Molecular dynamics simulations of pyrophyllite edge surfaces: Structure, surface energies, and solvent accessibility,” *Clays Clay Miner*, vol. 63, no. 4, 2015, doi: 10.1346/CCMN.2015.0630403.

[33] S. Plimpton, “LAMMPS-large-scale atomic/molecular massively parallel simulator,” *Sandia National Laboratories*, vol. 18, 2007.

[34] Z. Fan, Y. Wu, X. Zhao, and Y. Lu, “Simulation of polycrystalline structure with Voronoi diagram in Laguerre geometry based on random closed packing of spheres,” *Comput Mater Sci*, vol. 29, no. 3, 2004, doi: 10.1016/j.commatsci.2003.10.006.

[35] L. Momenzadeh, B. Moghtaderi, X. F. Liu, S. W. Sloan, I. V. Belova, and G. E. Murch, “The Thermal Conductivity of Magnesite, Dolomite and Calcite as Determined by Molecular Dynamics Simulation,” *Diffusion Foundations*, vol. 19, 2018, doi: 10.4028/www.scientific.net/df.19.18.

[36] S. Mahendran, P. Carrez, S. Groh, and P. Cordier, “Dislocation modelling in Mg2SiO4 forsterite: An atomic-scale study based on the THB1 potential,” *Model Simul Mat Sci Eng*, vol. 25, no. 5, 2017, doi: 10.1088/1361-651X/aa6efa.

[37] A. I. Jewett, Z. Zhuang, and J.-E. Shea, “Moltemplate a Coarse-Grained Model Assembly Tool,” *Biophys J*, vol. 104, no. 2, 2013, doi: 10.1016/j.bpj.2012.11.953.

[38] A. H. Ibrahim, P. Kumam, A. Kamandi, and A. B. Abubakar, “An efficient hybrid conjugate gradient method for unconstrained optimization,” *Optim Methods Softw*, vol. 37, no. 4, 2022, doi: 10.1080/10556788.2021.1998490.

[39] O. Hubert, “Multiscale magneto-elastic modeling of magnetic materials including isotropic second order stress effect,” *J Magn Magn Mater*, vol. 491, 2019, doi: 10.1016/j.jmmm.2019.165564.

[40] E. N. Borodin, A. A. Gruzdkov, A. E. Mayer, and N. S. Selyutina, “Physical nature of strain rate sensitivity of metals and alloys at high strain rates,” in *Journal of Physics: Conference Series*, 2018. doi: 10.1088/1742-6596/991/1/012012.

[41] A. K. Subramaniyan and C. T. Sun, “Continuum interpretation of virial stress in molecular simulations,” *Int J Solids Struct*, vol. 45, no. 14–15, 2008, doi: 10.1016/j.ijsolstr.2008.03.016.

[42] L. Pei *et al.*, “Effect of Temperature on Deformation and Fracture Behaviour of Nanostructured Polycrystalline Ni Under Tensile Hydrostatic Stress by Molecular Dynamics Simulation,” *J Nanosci Nanotechnol*, vol. 19, no. 5, 2018, doi: 10.1166/jnn.2019.15890.

[43] N. M. della Ventura *et al.*, “Response of magnesium microcrystals to c-axis compression and contraction loadings at low and high strain rates,” *Acta Mater*, vol. 248, 2023, doi: 10.1016/j.actamat.2023.118762.

[44] D. L. Goble and E. G. Wolff, “Strain-rate sensitivity index of thermoplastics,” *J Mater Sci*, vol. 28, no. 22, 1993, doi: 10.1007/BF00365009.

[45] Z. Ma, R. Pathegama Gamage, and C. Zhang, “Effects of temperature and grain size on the mechanical properties of polycrystalline quartz,” *Comput Mater Sci*, vol. 188, 2021, doi: 10.1016/j.commatsci.2020.110138.

[46] S. J. Blott and K. Pye, “Gradistat: A grain size distribution and statistics package for the analysis of unconsolidated sediments,” *Earth Surf Process Landf*, vol. 26, no. 11, 2001, doi: 10.1002/esp.261.

[47] R. Ajalloeian, H. Mansouri, and E. Baradaran, “Some carbonate rock texture effects on mechanical behavior, based on Koohrang tunnel data, Iran,” *Bulletin of Engineering Geology and the Environment*, vol. 76, no. 1, 2017, doi: 10.1007/s10064-016-0861-y.

[48] Z. Meng and J. Pan, “Correlation between petrographic characteristics and failure duration in clastic rocks,” *Eng Geol*, vol. 89, no. 3–4, 2007, doi: 10.1016/j.enggeo.2006.10.010.

[49] E. Eberhardt, B. Stimpson, and D. Stead, “Effects of grain size on the initiation and propagation thresholds of stress-induced brittle fractures,” *Rock Mech Rock Eng*, vol. 32, no. 2, 1999, doi: 10.1007/s006030050026.

[50] J. A. Garber and A. V. Granato, “Fourth-order elastic constants and the temperature dependence of second-order elastic constants in cubic materials,” *Phys Rev B*, vol. 11, no. 10, 1975, doi: 10.1103/PhysRevB.11.3998.

[51] I. Suzuki, O. L. Anderson, and Y. Sumino, “Elastic properties of a single-crystal forsterite Mg2SiO4, up to 1,200 K,” *Phys Chem Miner*, vol. 10, no. 1, 1983, doi: 10.1007/BF01204324.

[52] Y. Tang, W. Yin, and S. Kelebek, “Molecular dynamics simulation of magnesite and dolomite in relation to flotation with cetyl phosphate,” *Colloids Surf A Physicochem Eng Asp*, vol. 610, 2021, doi: 10.1016/j.colsurfa.2020.125928.

[53] M. Wolthers, D. Di Tommaso, Z. Du, and N. H. De Leeuw, “Calcite surface structure and reactivity: Molecular dynamics simulations and macroscopic surface modelling of the calcite-water interface,” *Physical Chemistry Chemical Physics*, vol. 14, no. 43, 2012, doi: 10.1039/c2cp42290e.

[54] L. Guldris Leon and M. Bengtsson, “Selective Comminution Applied to Mineral Processing of a Tantalum Ore: A Technical, Economic Analysis,” *Minerals*, vol. 12, no. 8, 2022, doi: 10.3390/min12081057.